# Copyright Warning & Restrictions

The copyright law of the United States (Title 17, United States Code) governs the making of photocopies or other reproductions of copyrighted material.

Under certain conditions specified in the law, libraries and archives are authorized to furnish a photocopy or other reproduction. One of these specified conditions is that the photocopy or reproduction is not to be "used for any purpose other than private study, scholarship, or research." If a, user makes a request for, or later uses, a photocopy or reproduction for purposes in excess of "fair use" that user may be liable for copyright infringement,

This institution reserves the right to refuse to accept a copying order if, in its judgment, fulfillment of the order would involve violation of copyright law.

Please Note: The author retains the copyright while the New Jersey Institute of Technology reserves the right to distribute this thesis or dissertation

Printing note: If you do not wish to print this page, then select "Pages from: first page # to: last page #" on the print dialog screen

# COMPUTATION OF COLLISION PARAMETERS OF SPHERES BY COMPUTER VISION

by
Sumit Sen

A Thesis
Submitted to the Faculty of
New Jersey Institute of Technology
in Partial Fulfilment of the Requirements for the Degree of
Master of Science
Depertment of Mechanical Engineering
October 1992

**APPROVAL PAGE**

**Computation of Collision Parameters of Spheres by Computer Vision**

**by**

**Sumit Sen**

---

Dr. Rajesh N. Dave, Thesis Advisor

Assistant Professor of Mechanical Engineering, NJIT

---

Dr Anthony D. Rosato, Committee Member

Assistant Professor of Mechanical Engineering, NJIT

---

Dr. Ian S. Fischer, Committee Member

Associate Professor of Mechanical Engineering, NJIT

**ABSTRACT**

**Computation of Collision Parameters of Spheres by Computer Vision**

**by**
**Sumit Sen**

Collision parameter evaluation of rigid spherical particles requires estimation of pre- and post-impact position, velocity and angular velocity vectors of colliding particles. A three dimensional experimental technique is devised where the instantaneous position and orientation of the particles are determined by analyzing frames obtained through high speed video imaging system. Since the image obtained is two dimensional, a mirror setting is designed to capture two orthogonal views of collision in order to estimate motion in depth. The translational velocity vector is determined from the position information extracted through application of available image analysis techniques over two time frames of digitized image. The angle and the axis of rotation between two time frames is determined by tracking a few randomly marked feature points on the spheres. In order to reduce the effect of error involved in the coordinate measurement in rotation estimation, a least square fitting of the set of three dimensional feature points is employed. The technique performed satifactorily in rotation vector estimation. The method developed here is applied to a set of experimental data for computation of collision parameters. Preliminary results indicate a need for improving the accuracy of position measurement.

## BIOGRAPHICAL SKETCH

**Author:** Sumit Sen

**Degree:** Masters of Science in Mechanical Engineering

**Date:** October, 1992

**Undergraduate and Graduate Education:**

- Master of Science in Mechanical Engineering
  New Jersey Institute of Technology, Newark, NJ, 1992

- Bachelor of Mechanical Engineering
  Jadavpur University, Calcutta, India, 1985

**Major:** Mechanical Engineering

This thesis is dedicated to

my beloved parents

## ACKNOWLEDGMENT

The author wishes to express his sincere gratitude to his supervisor, Assistant Professor Dr. Rajesh N. Dave, for his valuable guidance, friendship and moral support throughout this research. It has been an exhilarating experience working under his guidance.

A hearty appreciation to Dr. Anthony D. Rosato for the timely support with technical material , constructive criticism and suggestions.

Special thanks to Dr. Ian S. Fisher for devoting his precious time in reviewing this work and providing suggestions and encouragement.

The author is grateful to the Mechanical Engineering Department for providing financial support throughout this work.

The author acknowledges the help and support received from fellow researchers Mr. John Caesar, Mr. Jerry Volcy and Ms. Kimberly Hrnciar.

And finally, a thank you to Joe Glaz and Dave Singh for fabricating the experimental setup.

**TABLE OF CONTENTS**

**Page**

## LIST OF TABLES

**Table** **Page**

## LIST OF FIGURES

# CHAPTER 1
# INTRODUCTION

## 1.1 Background and Motivation

Experimental study in the field of particle collision has been impaired due to the constraints in tracking kinematics of particle in free space. In the past only two dimensional study of collision parameters analysis were carried out. The outcome of the study has widespread applications in many particle flow phenomena such as industrial solid handling, pharmaceuticals, plastics, sludge, slurries and natural geological flow [1]. All particle flow phenomena are very complicated by the fact that the motion of particles, as it interacts with other particles and obstacles, are highly nonlinear and random in nature. As an alternative approach, computer simulation models of particle dynamics are developed in absence of experimental data where individual particle trajectory has been tracked for predicting the behavior over a wide range of conditions [2, 3, 4, 5, 6]. However, the results of these simulations are highly dependent on the input particle collisional properties i.e. coefficient of friction ( $\mu$ ), the normal coefficient of restitution ( $e$ ), the rotational coefficient of restitution ( $\beta$ )[7, 8, 9,10].

Experiments through which collisional particle properties can be obtained have been scarce. In order to better validate the theories substantiated by experiments, it is necessary to devise a three dimensional experimental technique to measure these properties for subsequent use in theoretical development, physical experiments and numerical simulation. Hard sphere is the simplest model used in computer simulation of granular particles. Here we study the three dimensional kinematics of two colliding spheres from which collisional behavior will be observed through a known

collision operator. The Kodak EktaPro 1000 video imaging system, a high speed motion analyzer is used to obtain images of two colliding spheres. These images will be processed to obtain the pre- and post- collision kinematic data of translation and spin velocity of the spheres. The ability to actually measure the spheres' angular velocity and the axis of rotation by tracking a few randomly marked feature points on each of the spheres through automatic image analysis is a challenging part of this experiment. To circumvent the problem due to limited resolution of the imager, presence of noise in the image and consequent error in the measurement of feature point coordinates, mathematically an over determined set of linear transformation equations are formed to estimate the angle and axis of rotation. The best way to deal with this situation is to use a least square error method so that the square of the error is minimized with respect to the nine parameters of the rotation matrix.

## 1.2 Inelastic Hard Sphere Collision Operator

Until recently, most of the particle simulation models and rough particle theories have not properly included the effect of friction in their collision operator. Lun and Savage [5] described a rough inelastic hard sphere collision model incorporating a rotational restitution coefficient ( $\beta$ ), defined as the ratio of post- and pre-collision of relative surface velocity ( $v_s$ ), analogous to normal coefficient of restitution ( $e$ ), the ratio of post- and pre-collision relative normal velocity ( $v_n$ ). According to their rough inelastic sphere model, two particles of diameter $\sigma$ having translational velocity $V_1$ and$V_2$ and angular velocity $\omega_1$ and $\omega_2$ respectively have a total relative velocity $g_{12}$ at their contact point just prior to collision givenby

$$g_{12} = V_1 - V_2 - \frac{\sigma}{2}(\hat{r}_{12} \mathbf{x} \omega_{12}) \tag{1.1}$$

where $\hat{r_{12}}$ is a unit vector from particle 1 to 2, $\omega_{12} = \omega_1 + \omega_2$ and $V_{21} = V_1 - V_2$. During the collision the component of velocity and angular velocity are changed such that,

$$\hat{r_{12}} \cdot V_{21}' = -e \, ( \hat{r_{12}} \cdot V_{21} ) \tag{1.2}$$

and

$$\hat{r_{12}} \times g_{12}' = -\beta \, (\hat{r_{12}} \times g_{12}) \tag{1.3}$$

where the prime indicates the post collision values. The normal coefficient of restitutions ( $e$ ) and the rotational coefficient of restitution ( $\beta$ ) are assumed constants in the range, $0 \leq e \leq 1$ and $-1 \leq \beta \leq 1$ where $\beta = -1$ being perfectly smooth, $\beta = 1$ perfectly rough and $\beta = 0$ corresponds to Campbell's rolling contact model.

When two particles collide, two contact states can be distinguished as (i) sliding, in which the the ratio of friction force to normal force i.e. the coefficient of friction ( $\mu$ ) remains constant (ii) rolling, where the friction force is zero [11]. As proposed by Walton[6] the adoption of the frictional collisional operator allows us to use a much more efficient hard sphere code that can predict the collision properties.

The algorithm below is taken from Walton [6] and is repeated here for clarity.

$$\hat{r_{ab}} = \frac{1}{\sigma} (r_b - r_a) \quad (at\ contact)$$

$$V_{ab} = V_b - V_a$$

$$v_n = V_{ab} \cdot \hat{r_{ab}}$$

$$V_n = V_{ab} \cdot \hat{r_{ab}} \cdot \hat{r_{ab}}$$

$$V_t = V_{ab} - v_n \cdot \hat{r_{ab}} = \hat{r_{ab}} \times (V_{ab} \times r_{ab})$$

$$V_s = V_t + \sigma/2 \cdot \hat{r_{ab}} \times (\omega_a + \omega_b)$$

$$k_s = \frac{V_s}{||V_s||}$$

$$v_s = V_s \cdot k_s$$

The equation of rolling solution is expressed as

$$-\frac{v_s'}{v_n'} = -\frac{\beta_0}{e}\frac{v_s}{v_n} \tag{1.4}$$

and the equation for the sliding solution line is given by

$$-\frac{v_s'}{v_n'} = -\mu\,(1+\frac{1}{e})\,(1+\frac{1}{k}) + \frac{1}{e}\frac{v_s}{v_n} \tag{1.5}$$

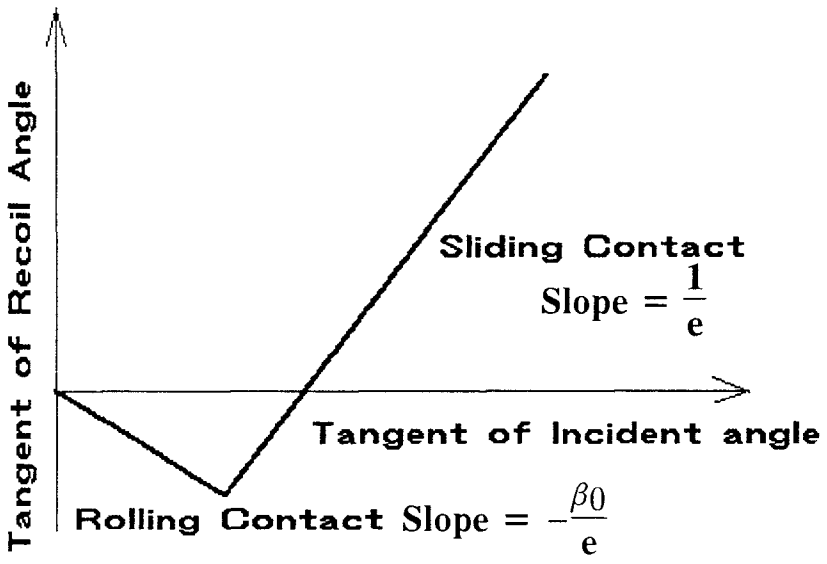


**Figure 1.** Theoratical Sliding and Rolling Solution from Walton[6].

If we plot the tangent of the recoil angle or pre-collision ratio normal to surface velocity ( $\frac{v_s}{v_n}$ ) vs tangent of the incident angle or the ratio of the post-collision normal to surface velocity ( $\frac{v_s'}{v_n'}$ ), the folling curve will be obtained. It may be noticed that if the curves can be developed experimentally the slope of the lines provide us all the collision parameter information.

## 1.3 Justification of Application of Computer Vision in Particle Motion Tracking

Vision is the most powerful sense that allows us to extract tremendous amounts of information about our surroundings and interact with the environment dynamically and intelligently. With numerous recent development in digital image processing researchers could impart a sense of vision to a machine through a computer. A great deal of useful information can be extracted from a time varying image sequences. The change in the environment can be manifested by a sequence of image frames and such the motion information of a dynamic scene (as seen through a camera) can be retrieved and utilized further by processing a sequence of digital images taken at different time instants.

Experimentally tracking the motion of single particle has been a tedious task until the recent introduction of video cameras and recording systems. Traditionally high speed motion picture cameras have been used to record the motion of the particles on a film and then developed the film and analyzed to study the phenomena of interest. This approach is very time consuming and costly. Moreover the information obtained by this method is not usable for the automatic motion analysis task using digital computer. Introduction of video cameras, recording devices and analog to digital image conversion technique has provided a fast efficient and more accurate method of particle motion tracking. Major advantage of video system includes immediate playback capability and easy interfacing facility to a digital computer.

If we are analyzing the visual image of a scene as seen through a camera, it is very difficult to extract the relative depths of various feature points and from a single frame. As the object move, the relative orientations of various feature points on the object change on the image plane. The shift in the image coordinate may allow us to recover relative depths of various feature points [13]. The relative motion of the

object in the scene gives rise to an apparent motion of the object in image sequence. If we assume the object remained fixed, two frames will constitute a stereo pair and transferring the frame of reference fixed on the camera can also enable us to determine the motion parameters of the object. However the accuracy of depth estimation through stereo triangulation is directly proportional to the the length of the base line [14, 15]. However the best solution is the coordinate of feature points in two orthogonal views.

It enables us to determine translation and rotation over the time period between two snap shots. For the estimation of the coordinate of the markers in each frame the application of various edge-detection (image processing) algorithms will be appropriate. Once the coordinate of each marker has been calculated in each frame, there remains the main problem of establishment of correspondence of each marker from one frame to other. Rangrajn and Shah [16] has defined the problem as, given n frames snapped at different instant of time and p points (features) in each frame, the problem of motion correspondence is to map a point in one frame to a point in the next frame such that both are the projection of the same point on the original object. Recent improvement in the logic of the algorithms has transformed the program robust enough to do automatic matching of each marked point from one frame to other.

Apart from this optical method, few of the alternative techniques to determine 2-dimensional and 3-dimensional position and velocity (linear and angular) of particles can be classified as following three groups, such as

(i) Direct measurement from field of view through X-ray or gamma ray where colliding particles should be X-ray sensitive and the experimental setup has to be X-ray transparent.

(ii) Remote detection by the emitted or reflected electromagnetic or sound wave from the tracer mounted on the colliding particles, include the use of (a) Radio isotope, which is very expensive and involves health hazard (b) Magnetic tracer, can be used with steel only (c) Ultrasound emitter is very expensive (d) Electro magnetic tracer hving radiosonde transmitter coupled with a set of receiving antenna communicating through magnetic induction can also be used. The position information is computed from phase or amplitude of the detected signal. However no metallic particle can be tested by this method. Since all the remote sensing techniques require a tracer to be imbedded on the particle which change the material property, consequently they are unsuitable for collision parameter analysis.

(iii) There are a few 'Probe techniques' for observing the behavior of particle motion like fibre optic probe and capacitance probe. In all these methods a probe has to be installed which causes obstacle to the motion. Therefore this method is unsuitable.

Though the list above is not exhaustive but all other methods are equally complicated, expensive or the scale of operation do match with the laboratory experimentation.

## 1.4 Thesis Outline

In the next chapter a brief review of previous work being done in application of image processing for tracking 2-dimensional and 3- dimensional particle motion has been presented. A brief survey of past work in the field of hard sphere inelastic collision model is also described.

Chapter 3 provides the detailed discussion of the required specification and an overview of the experimental setup discussing how two orthogonal views of the collision can be captured with the mirror setting and one camera. Here we discuss the various flexibility in the design of setup which takes care of all the input conditions necessary for successful experimentation.

Chapter 4 covers the sequential steps to be followed to recover the (x, y, z) coordinate of each marker with respect to world coordinate frame in each snapshot. Here we present the mathematical algorithm developed for determination of linear and angular velocity of each sphere in the time period between two subsequent image frames.

Chapter 5 discusses accuracy of the proposed mathematical algorithm in determining the linear and angular velocity using the camera system. Calibration of the proposed technique is done using simulated input data.

In Chapter 6 we have the outcome of the collision experiment and presents the inferences from the numerical results and conclusions we can draw from the experiment. An idea for improvement in future direction of research is also presented.

Appendix A discusses the mathematical derivations necessary for understanding the mechanics of particle collision. The solution expressions of the collision operator described here are taken from Walton[6] for the sake of completeness of experiment.

Appendix B gives us a brief description about the salient features of Kodak Ektapro1000 Camera and intesfied Imager system which plays an important role in this experiment.

Appendix C provides a brief discussion on Least square analysis of overdetermined system of equations.

# CHAPTER 2
# LITERATURE REVIEW

## 2.1 A Review of Development of The Collision Parameter Estimation

In the classical problem of impact when two rigid particles collide, the single most important feature is the effect of friction. Over an above the normal and rotational coefficient of restitution, the responce of the rigid bodies in oblique impact depend on the coefficient of friction. The role of the frictional force in the collision operator so far has not been properly studied in most of the past rough particle theories and their simulation models.

In kinetic theory models, similarities have been drawn between the dynamics of dense systems of colliding gas molecules and the shearing of granular material [2, 3, 4, 5,7,8]. But the inelastic nature of the collision in a sheared granular particle flow is in contrast to the assumption of nondissipative interactions in a dense gas. Berne treated rough disks and Veseley attempted partially rough Lennard-Jones spheres but didn't include energy losses due frictional or inelastic forces [17, 18].

In 1977 Maw et. al. performed 2-dimensional air-table experiments in which disks machined from spheres [11] were rebounded from rigid fixed block. While the results of these experiments were useful in substituting their modified Hertzian theory but this 2-dimensional technique can not be employed to obtain properties for particles to be used subsequently in granular flow experiments. Hawkins did a simulation study of frictional inelastic hard disks utilizing Goldsmith's collision operator [19] however no quantitative results have been reported [20]. Campbell

and Bernnen in 1985 utilized an inelastic rough disk model and experimented in two dimensions [21].

Of late, Drake et. al. [12] performed a quasi two dimensional experiment from which particle collision properties were computed. Here quantitative particle motion information during collision was obtained employing a combined procedure of collecting the image of the collision and manually digitizing frames together with the use of software to compute particle velocities and spins between collisions. Subsequent data analysis to obtain collision properties for use in particle dynamics simulations was restricted due to the interference of the wall.

Lun and Savage [5] described a rough inelastic collision model incorporating a property namely, rotational restitution coefficient, defined analogous to the normal direction coefficient of restitution but did not include the effect of friction [5]. Nakagawa [3] proposed a statistical theory of inelastic frictional disk collision operator similar to that used by Hawkins [20]. Walton and Braun [8] in their deformable particle model, allowed the effect of both inelasticity and frictional energy loss. Data was collected at very small time steps and subsequent integration of the motion of the equations are necessary which is computationally intensive [7]. Experiments through which three dimensional collisional particle property can be obtained have been scarce.

Walton [6] extended the disk collision operator of Hawkins or Nakagawa to 3-dimensions with additional features of coefficients of normal and rotational restitution ( $e$ & $\beta$ ) for contacts that are not continuously sliding during entire collision and a coefficient of sliding friction ( $\mu$ ) for sliding contact [6]. This three-parameter model can more accurately describe collision properties and can also be extended to represent Maw's [11] Hertz-Mindlin collision model between frictional elastic spheres. Detailed material properties e.g. coefficient of friction ( $\mu$ ), normal and

rotational restitution coefficients ( $e$ , $\beta$ ) are necessary in the calculations of stresses , viscosity and granular flow temperature. Therefore it is necessary to devise a three dimensional experimental technique whereby these properties can be measured.

## 2.2 Role of Image Processing in Particle Motion Analysis

Application of computer vision in estimation of particle motion has been a challenging and active topic of research for more than a decade [22, 23, 24]. It may seem that processing a sequence of images would be much more complex than processing a single image. However a great deal of information about the particle motion can be derived from a sequence of images that may not be available from a single image. Widespread techniques and image processing algorithms are already available for processing a sequence of images to derive these information. Existence and uniqueness of the solution procedures and results are also available too.

But the past research on motion analysis through image processing was mainly restricted to 2-dimensional motion. Methods for 2-dimensional motion estimation are relatively well known [25] - [32]. This is because interpretation of images of objects moving in 3-dimensions is much more complicated than two-dimensional motion. Rotation in space is about a line in three dimensional space where as rotation in plane is about a point in the plane. In addition, part of an object can disappear from view as a result of rotation in space however rotation in a plane dose not cause an object to occlude itself. Moreover the movement in depth is difficult to compute and explain.

Analyzing the 3-dimensional image requires intricate mathematical formalization. Psychologists have studied movement in terms of texture gradients and often

other cues that aid human depth perception (Gibson [33] and Braunstein[34]). These psychologists use brightness of image-points on the surface of the objects to study movement in depth. Roberts [35] also used surface points on a rigid object to determine object depth. We know the 3-dimensional relationship of points on a rigid object do not change over time. Consequently, changes in the 2-dimensional spatial relationship of object surface points between images must be caused by the relative movement between the camera and the object being imaged. The 3-dimensional motion estimation from two images with single camera, when the surface of the object is not restricted to any particular shape, requires solution of nonlinear equations with iterative search unless very special assumptions are made to simplify the problem for example: the fixed axis assumption [36] which is satisfied only by those movements consisting of translation and rotation about fixed axis over several frames . The parallel projection assumption [36, 37] which approximately calculates the motion parameters if the object far away from the camera. From the coordinate of the image points and the surface geometry, it is possible to derive the nonlinear equations of the motion parameters. The next problem is the closed form solution of the non-linear equations. Therefore it requires, first, how many feature points correspondence are necessary for uniqueness of the solution. Second, how to make good initial guess to reduce the computations in iterative search. In solving nonlinear equations iteratively the computational complexity is enormous since global search is necessary. Unless the initial guess is good enough the local minimum obtained will not be the global minimum. For the uniqueness problem , it is generally tried to get the number of equations to be equal to the number of unknown [38, 39].

Tsai and Huang [40] formulated this problem so as to obtain linear equations and proposed that eight point correspondences can uniquely determine the motion parameters up to a scale factor for translation. They assumed that the focal length of the lens is not known explicitly and the translation includes a scale factor. The

motion parameters can be subsequently determined by computing the singular value decomposition (SVD) of the 3 x 3 matrix containing essential parameters. They have shown that computing the least-square solution a system n linear equation with 8 unknowns (n is the number of point correspondences used and is greater than or equal to 8) and the singular value decomposition of a 3 x 3 matrix. However their results show that 3% perturbation (error) in the estimation of coordinates will result in 101.8% error in the estimation of motion parameters.

In studies involving binocular vision, (i.e. two cameras or eyes separated by the known distance apart) is known as 'disparity' of the same point in two images. A simple triangular formulation gives the depth of point in this case. Here the problem of determination of depth is analogous to the stereo photogrammetry problem. Thus the change of position between images of points on a rigid object's surface can be used to formalize the problem of determining the three dimensional movement of objects in space [14].

Castro and Morandi [41] has shown a finite fourier transform method of image registration based on a conventional correlation of brightness between two versions of the same image, being realigned, can be employed for motion estimation. This method can perform well against correlated noise and disturbances such as those encountered with nonuniform, time varying illumination. This correspondence can be used to cover both translation and rotational movement. Weng, Huang and Ahuja proposed a locally constant angular momentum model for estimation of 3-dimensional motion from the measurement of projective positions. It is assumed that the angular momentum is constant over a short interval and the trajectory of the center of rotation is expressed is described as a polynomial [42]. Whon [1989] proposed that the 3-dimensional velocity can modeled as an arbitrary order power series. Regression relation between unknown parameters and measurements from noisy

images was derived and the optimum estimate based on maximum likely hood is calculated in batch approach [43]. However this method is unsuitable if there is abrupt change in motion [e.g. collision] of the object in the scene, as a result the order of the power series may not match the model exactly. Two types of mismatch commonly encountered are (i) parameter mismatch due to sudden change in motion parameters and (ii) under modelling occurs when the order of the power series of the trajectory model is less than the actual motion. In order to circumvent this problem Su and Whon proposed a recursive approach to speed up the motion parameter estimation and a 'Finite Lifetime Alternately Triggered Multiple Model Filter (FLAT MMF)' as a solution against possible model mismatch [44].

Contribution by others in the field of motion analysis include Ullman[22], reports that if point correspondences are known, the 3-dimensional spatial location of four co-planer points can be uniquely determined from just three projections. Badler [45] used a spherical projection model and was able to predict the point positions in succeeding images of translating objects. Lawton [46] reports that a solution exists for four non-coplaner points can be uniquely determined from just three perspective projections and adds that five points are needed for two perspective projections, the equations are nonlinear and solution obtains through iterative search.

There are number of image processing algorithms available for separating out various edges of the objects in an image, namely Canny's operator [47] , Hough transform technique [48], Fuzzy shell clustering technique for center detection of circle [49] etc. After extracting feature points on object surface in each image the problem reduces to establish the correspondence of those points between consecutive images. By correspondence problem we mean the mapping that takes any feature point from one image to the image of the same feature point in the next frame. This is a difficult task since an image may have more than one moving feature points

and thus many points to choose from . The correspondence is further complicated by the by the disappearance of the points on an object surface due occlusion from the other object or self occlusion since the point rotate out of view , shadows and the noise in the image etc. Rangrajan and Shah has developed an algorithm where the constraint is used to limit the search space which is termed as 'Proximal uniformity constraint', can be employed to establish the motion correspondence of feature points from one frame to the other provided the initial correspondence of feature points between first two frames are known [50].

Once the correspondence of feature points has been established we attempt to analyze the motion. Now, how the motion can be represented ? Homogeneous coordinates are an elementary means of representation movement since a 4 x 4 matrix can represent any translation and rotation. Given these two elementary motion matrices it is possible to represent any motion of an object in space. A theorem from classical mechanics by Coffin[51] established that any motion, including the rotation within rotation problem (even n axis of rotation) can be decomposed into one rotation and one translation. The translation component of the motion can be estimated by noting the change in the center of the object during successive time instant [52]. Therefore the problem reduces to the estimation of the rotation matrix. Ideally it can be determined by correspondence of three feature points between two frames. However inaccuracy in the estimation of feature points may occur due to the sampling error, human error, modelling error and instrument errors. There are various error elimination methods available namely least square error, total least square estimator and least median square techniques.

Chaudhuri and Chatterjee [1990] proposed evaluation of rotation parameters by considering the invariance of principle moments of the object in successive frame [52]. An invariant is any numeric feature that does not change when one or more of

the following operations are performed on an object. For example translation, rotation, reflection and scaling. They have shown that total least square method is found to perform better as to conventional LS estimator in the presence of errors in feature point correspondence. However they used subset correspondence instead of individual feature point correspondence. Once the rotation and translation matrices has been determined, they can be multiplied together to form one matrix useful for predicting the subsequent 3-dimensional position of the object. In addition to representing motion, a 4x4 matrix in homogeneous coordinates can be used to model the projection of object points on to the focal plane of the camera.

# CHAPTER 3
# EXPERIMENTAL SETUP

## 3.1 Specification of The Experimental Setup

When two particles collide [11], two contact states can be distinguished as: sliding, in which the ratio of friction to normal force is equal to $\mu$, and rolling, in which the friction force is zero. It can be shown, while colliding , if the particles dissipates sufficient energy so that two particles lose all relative tangential velocity, the frictional force become zero, they roll over each other. This sudden change in the tangential force which causes the transition from sliding contact to rolling contact can be achieved by allowing two spheres to collide with gradually increasing the ratio of tangential to normal velocity before collision. The objective of this research is to measure values of $e$ , $\beta$ and $\mu$ by colliding two spheres in space and computing their post collisional kinematics. The rolling and sliding solutions [6], can be expressed as

$$-\frac{v_s'}{v_n'} = -\frac{\beta_0}{e}\frac{v_s}{v_n} \tag{3.1}$$

and

$$-\frac{v_s'}{v_n'} = -\mu\,(1+\frac{1}{e})\,(1+\frac{1}{k}) + \frac{1}{e}\,\frac{v_s}{v_n} \tag{3.2}$$

where $e$ & $\beta_0$ represent the translational and rotational coefficient of restitution; $v_s/v_n$ and $v_s'/v_n'$ are the ratio of tangential to normal velocity before and after collision, $\mu$ is the co-efficient of friction and $k$ is a constant $=2/5$ for sphere. If we plot $v_s'/v_n'$ vs $v_s/v_n$ which is equivalent to the plot of tangent of the effective recoil angle $\Psi 1$vs the tangent of the effective incidence angle $\Psi 2$ as shown in figure1.

rotational and liear coefficient of restitution ($\beta$ and $e$ ) will be calculated from pre- and post-collision value of $v_s$ and $v_n$ in each session of experiment. In order to check the above theory the experimental setup should have certain flexibility and conform the following specification.

(i) There should have the facility to allow two spheres to collide at any desired angle of incidence and the post-collision motion of the spheres should be unrestricted.

(ii) There should be virtually frictionless condition during collision so that the motion of the spheres are not impaired by the effect of friction

A sketch of the experimental setup is shown below in Figure 2.

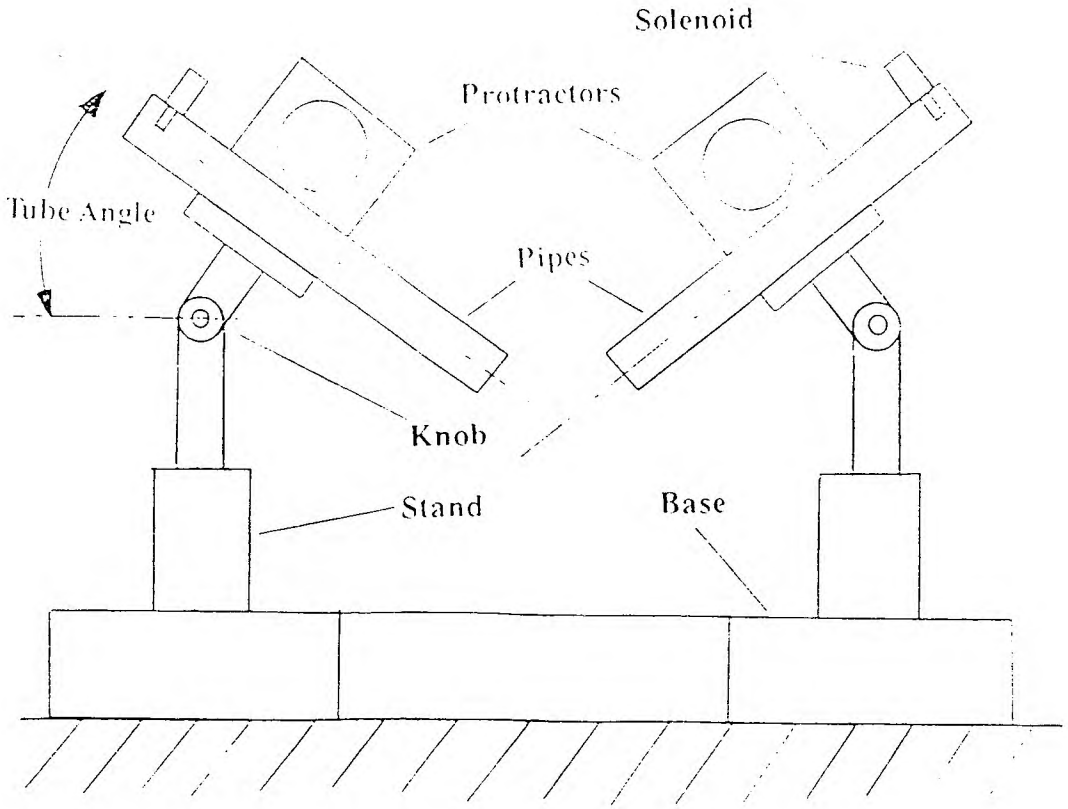


**Figure 2** Experimental Set-up for Sphere Collision

(iii) The experimental setup has to ensure that two spheres must collide at the specified angle as desired.

(iv) The motion of the spheres before and after collision should lie on one plane. The plane should be parallel to the image sensor of the camera.

How these conditions are fulfilled are explained below.

## 3.2 Operations and Control of The Experimental Setup

Two stands shown on the figure2 can rotate about their axis on the base of the frame. The tube-holders mounted on the stand can rotate about the axis perpendicular to the axis of the respective tube. This enables us to make any desired angle between the axes of two tubes which in turn will make two balls collide at any desired angle. The spheres are held at the top of the tubes and control of the releasing system of the spheres is accomplished by designing a triggering mechanism by using translational solenoids. The spheres are held at the top of the tube by the protruding shaft of the solenoids.

An interface is established between a computer and the sphere projectile triggering mechanism through a electrical relay which receives a signal from the computer and turns on the 24 volt power supply to the solenoids. The shafts of the solenoids are pulled up at the same instant, consequently both the spheres are released at the same instant, which in turn ensures the collision of the spheres at the desired angle. Two rulers are pasted on tubes and the tubes can slide on the tube-holders. Thus we can measure the length of travel of the spheres in the tubes which in turn controls the velocity of the spheres immediate before collision. The

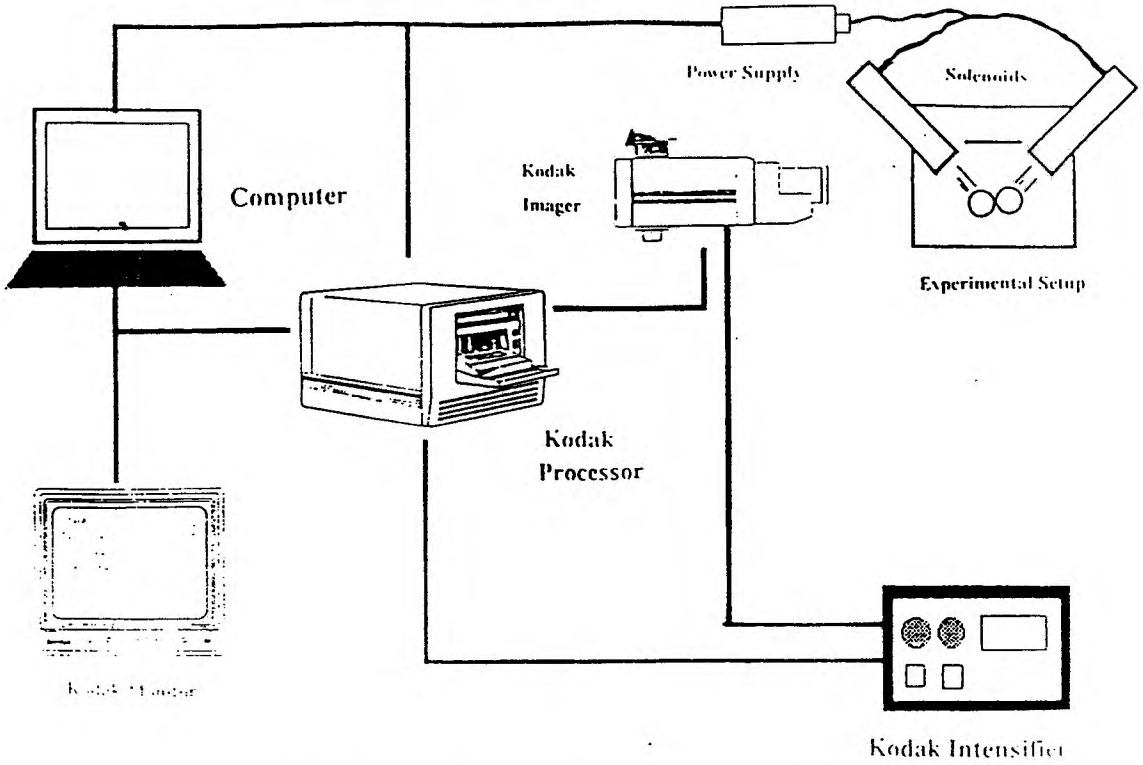


**Figure 3** Control Diagram for the Experimental Set-up

spheres are in free flight upon release from the tubes and collide in space. Therefore the effect of air friction is negligible. However due to the gravitational effect, upon release from the tubes the motion of the spheres, instead of linear, tend to be parabolic. Consequently the angle of incidence of the colliding spheres is different from the desired angle. Therefore the tubes are to be set such that the collision occurs immediately upon released from the tubes thereby minimize the effect of gravity.

Kodak Ektapro1000 high speed video imaging system is used to capture the image of the collision. The whole experiment has been automated such that the control of the exact timing of collision and simultaneous recording of the event has been achieved by a single command from a computer. A diagram of the communication of signal and image data is shown next page. To evaluate the collisional parameters here we need to measure the position of both the spheres $r_a$ and $r_b$, in

each frame and translational velocity of each of the spheres $V_a$ and $V_b$ , angular velocity of each of the spheres $\omega_a$ and $\omega_b$ respectively between two frames. Thus the pre- and post kinematic trajectory information of two spheres colliding in space will be obtained. These data will be processed and to be substituted in the following equations which defines the normal ($e$) andtangential ($\beta$ ) coefficients of restitution.

$$\hat{r_{ab}} \cdot V_{ba} = -e \cdot (\hat{r_{ab}} \cdot V_{ba}) \tag{3.3}$$

and

$$\hat{r_{ab}} \times g_{ab}' = -\beta \cdot (\hat{r_{ab}} \times g_{ab}) \tag{3.4}$$

where primed and unprimed symbols are the values immediately after and before a collision respectively and $\hat{r_{ab}}$ is unit vector connecting the centers of sphere $a$ and $b$ at contact. The $g_{ab} \equiv v_{ba} - \sigma/2\,(\hat{r_{ab}} \times \omega_{ab})$ is total relative velocity of the contact point and $\omega_{ab} \equiv \omega_\alpha + \omega_\beta$. The basic idea of this method is to experimentally determine the rolling and the sliding solution curves as depicted in Figure 1. This will be acocomplished by computing values of $v_s/v_n$ before and after collision. By making use of the equations 3.1 and 3.2, which define these two solutions, it is also possible to calculate the values of normal and rotational coefficient of restitution ($e$ and $\beta$ ) and the coefficient of friction ($\mu$) from the slope of these curves.

# CHAPTER 4
# DETERMINATION OF LINEAR AND ANGULAR VELOCITY OF THE SPHERES

## 4.1 Estimation of ( $X, Y, Z$ ) Coordinate of The Feature Points

Analysis of generalized motion parameters involves the estimation of translation and rotation of spheres. The translational motion is to be evaluated by observing the change in the coordinate of the sphere centers between two time frames. The rotational motion analysis requires the determination of 3-dimensional coordinate of a few randomly marked feature points on the spheres in each frame and establishing the correspondence of those feature points between two subsequent frames. This will be achieved according to the following few steps.

When two spheres are in motion before or after the collision, if they do not remain on one single plane in pre- or post-impact state, it is termed as 3-dimensional collision. To determine the position of the sphere we adhere to following sequential steps

(1) Set two coordinate frames

(a) Screen coordinate frame i.e. the 2-dimensional coordinate frame of the monitor of the Kodak Ektapro 1000 imager.

(b) World coordinate frame i.e. the frame set on the world visible by the camera positioned at the lower left corner of the image frame

(2) It is assumed that the x-y plane of the world coordinate frame is parallel to the image sensor of the camera. Therefore the 2-dimensional screen coordinate frame is oriented parallel to the x-y plane of the world coordinate frame. We find the correlation between screen coordinate and world coordinate frame. This is basically the scale

factor for x and y direction. This enables us to calibrate imager to the world coordinate system

(3) Since there is only one camera therefore to collect two orthogonal views of the collision, a mirror is set at 45 degree angle with the x-y plane of the of the world co-ordinate frame. A schematic diagram of the operation is shown below. following

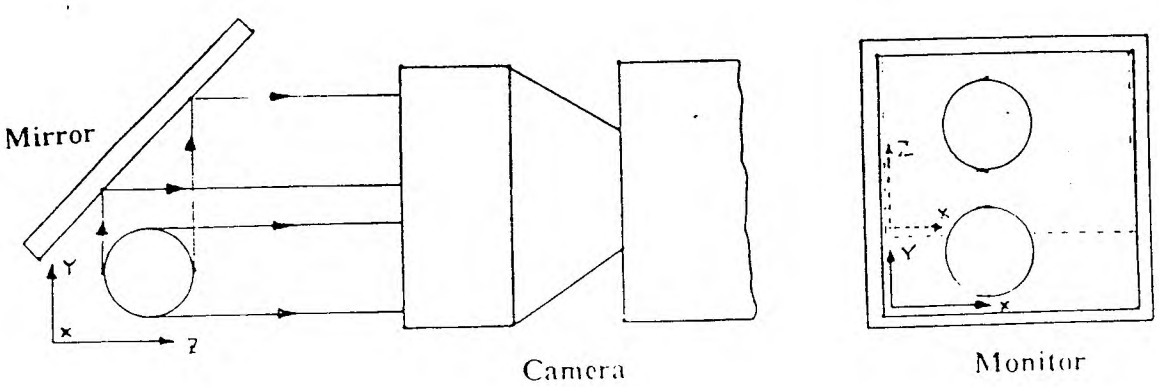


**Figure 4** Mirror Set-up for Two Orthogonal Images

this scheme we can find the perspective projection of the spheres on x-y and x-z plane of the spheres on the top and bottom half of the monitor.

(4) Camera collects the image of collision and stores that in the tape.

(5) We select two frames before collision where at least same three or more feature points are visible in bottom half of both the frames .

**From the first frame of the image**

(6) Determine the screen coordinate of the feature points $(x_i, y_i)$ where i = 1 to n the number of feature points and the coordinate of the center of each sphere $(x_c, y_c)$. Convert the screen co-ordinate of these feature points to world co-ordinate and determine the z co-ordinate from the following equation

$$z_i = \sqrt{r^2 - (x_i - x_c)^2 - (y_i - y_c)^2}$$

where i = 1 to n for each of the feature points. Thus the world coordinate of those feature points say $(X_{ai}, Y_{ai}, Z_{ai})$. Similarly the coordinate of the feature points on other sphere is determined as $(X_{bi}, Y_{bi}, Z_{bi})$

(7) Determine the center of the sphere in screen coordinate and from scale factor find the world coordinate of the same say $(X_{ac}, Y_{ac}, Z_{ac})$ and $(X_{bc}, Y_{bc}, Z_{bc})$ respectively

(8) Since the spheres are rotating about an axis passing through the cetroid i.e. the center opf the spheres therefore we transfer the world coordinate frame to the center of the sphere and find the coordinate of the feature points in terms of the transferred world coordinate frame $X_{ai}-X_{ac}, Y_{ai}-Y_{ac}, Z_{ai}-Z_{ac}$ and $X_{bi}-X_{bc}, Y_{bi}-Y_{bc}$, $Z_{bi}-Z_{bc}$ for i = 1 to n; number of feature points on the sphere.

**From the second frame of the image**

(9) Repeat the steps (5) , (6) and (7) on the second frame and find out coordinate of those feature points on each sphere in terms of the world coordinate frame transferred to the respective center of the sphere.

(10) The linear translation of the spheres are represented by the distance of the center of each sphere in two frames. The center of the spheres are represented in terms of world coordinate frame

(11) Select two frames just after collision where same feature points are visible in lower half of both the frames.

(12) Repeat steps (5) , (6) , and (7) on both the frames before and after motion

(13) The rotation of the spheres can be represented by rotation transformation Matrix

$$R = \begin{bmatrix} N_x & O_x & A_x & 0 \\ N_y & O_y & A_y & 0 \\ N_z & O_z & A_z & 0 \\ 0 & 0 & 0 & 1 \end{bmatrix}$$

If we select three feature points , the position of the feature points in two frames before and after motion will give us nine equations and solving them we get nine

unknown elements of matrix R. The axis and the amount of rotation w.r.t. the world coordinate frame transferred to the center of each sphere.

**(14)** The linear translation and rotation of the ball after collision can be found out following the step (10 ), (11) and (12).

**(15)** From the translation and rotation before and after collision; the linear and angular velocity and the linear and rotational coefficient of restitution can be evaluated .

## 4.2 Determination of Linear Velocity

The procedure for determination of linear velocity relatively simple. The position of the centroid (i.e. the center) of the sphere at the first frame i.e. time $t_1$ is estimated as $(x_1, y_1, z_1)$ with respect to the fixed world coordinate frame. The change in the position of the centroid to $(x_2, y_2, z_2)$ in the next frame at tme $t_2$ enables us to displacement $\Delta s$

$$\Delta s = \sqrt{((x_2 - x_1)^2 + (y_2 - y_1)^2 + (z_2 - z_1)^2)} \tag{5.1}$$

and the linear velocity is evaluated as

$$V = \Delta s / \Delta t \tag{5.2}$$

where time elapsed between two frames $\Delta t = t_2 - t_1$. However we have to evaluate the instantaneous velocity at two frames before and after collision. Therefore we calculate the velocity of the spheres between two cosecutive pair of frames, all are at equal intervals and take the average to evaluate the instantaneous velocity at the intermediate frame.

## 4.3 Angular Velocity Determination By Feature Points Correspondence

To determine the angular velocity $\omega$ , it requires the evaluation of the angle and the axis of rotation of the sphere between two time instant. If the sphere has rotated an angle $\theta$ between time $t_1$ and $t_2$ about an axis passing through the center of the sphere having the direction cosines as $K_x$ , $K_y$ and $K_z$ , the angular velocity $\omega$ is estimated as

$$\omega = \theta / \Delta t \tag{5.3}$$

where $\Delta t = t_2 - t_1$ and the axis of rotation is represented as $K_x i + K_y j + K_z k$

To determine the angle and the axis of rotation we have to evaluate the 3 x 3 rotation matrix $[R]$ that can best express the transformation. The columns of $[R]$ are mutually perpendicular to each other and expressed as

$$R = \begin{bmatrix} N_x & O_x & A_x & 0 \\ N_y & O_y & A_y & 0 \\ N_z & O_z & A_z & 0 \\ 0 & 0 & 0 & 1 \end{bmatrix} \tag{5.4}$$

We will now develop the transformation matrix representing a rotation around an arbitrary vector passing through the center of the sphere. In order to construct the matrix we will imagine that $k$ is the $z-$axis unit vector of a coordinate frame $C$, where

$$C = \begin{bmatrix} N_x & O_x & A_x & 0 \\ N_y & O_y & A_y & 0 \\ N_z & O_z & A_z & 0 \\ 0 & 0 & 0 & 1 \end{bmatrix} \tag{5.5}$$

$$k = a_x i + a_y j + a_z k \tag{5.6}$$

Rotating around the vector $k$ is then equivalent to rotating around the z axis of the frame$C$

$$Rot(k, \theta) = Rot(c_z, \theta) \tag{5.7}$$

If we are given a coordinate frame T described with respect to the reference coordinate frame, we can find a frame X which describes the same frame with respect to frame $C$ as

$$T = C \,.\, X \tag{5.8}$$

where $X$ describes the position of $T$ with respect to frame $C$. Solving for $X$ we obtain

$$X = C^{-1} \,.\, T \tag{5.9}$$

Rotating $T$ around $k$ is equivalent rotating $X$ around the $z-$axis of frame $C$

$$Rot\ (k\ ,\theta)\ T = C\ Rot\ (z\ ,\theta)\ X \tag{5.10}$$

$$Rot\ (k\ ,\theta)\ T = C\ Rot\ (z\ ,\theta)\ C^{-1}\ T \tag{5.11}$$

Thus we get

$$Rot\ (k\ ,\theta) = C\ Rot\ (z\ ,\theta\ )\ C^{-1} \tag{5.12}$$

However, we have only $k$, the $z-$axis of the frame $C$. By expanding the above equation we will discover that $C \,.\, Rot\ (z\ ,\theta) \,.\, C^{-1}$ is function of $k$ only. Multiplying $Rot\ (z\ ,\theta)$ on the right by $C^{-1}$, we obtain

$$Rot\ (z\ ,\theta) \,.\, C^{-1} = \begin{bmatrix} Cos\theta & -Sin\theta & 0 & 0 \\ Sin\theta & Cos\theta & 0 & 0 \\ 0 & 0 & 1 & 0 \\ 0 & 0 & 0 & 1 \end{bmatrix} \begin{bmatrix} n_x & n_y & n_z & 0 \\ o_x & o_y & o_z & 0 \\ a_x & a_y & a_z & 0 \\ 0 & 0 & 0 & 1 \end{bmatrix}$$

Therefore by multiplication, we get

$$Rot\ (z\ ,\theta) \,.\, C^{-1} = \begin{bmatrix} n_xCos\theta - o_xSin\theta & n_yCos\theta - o_ySin\theta & n_zCos\theta - o_zSin\theta & 0 \\ n_xSin\theta + o_xCos\theta & n_ySin\theta + o_yCos\theta & n_zSin\theta + o_zCos\theta & 0 \\ a_x & a_y & a_z & 0 \\ 0 & 0 & 0 & 1 \end{bmatrix} \tag{5.13}$$

Premultiplying the above by

$$C = \begin{bmatrix} N_x & O_x & A_x & 0 \\ N_y & O_y & A_y & 0 \\ N_z & O_z & A_z & 0 \\ 0 & 0 & 0 & 1 \end{bmatrix}$$

Thus we obtain

$$C.Rot(z,\theta).C^{-1} = \begin{bmatrix} n_x n_x Cos\theta - n_x o_x Sin\theta + n_x o_x \sin\theta + o_x o_x \cos\theta + a_x a_x \\ n_y n_x Cos\theta - n_y o_x Sin\theta + n_x o_y \sin\theta + o_y o_x \cos\theta + a_y a_x \\ n_z n_x Cos\theta - n_z o_y Sin\theta + n_x o_z Sin\theta + o_z o_x Cos\theta + a_z a_x \\ 0 \end{bmatrix}$$

$$\begin{bmatrix} n_x n_y Cos\theta - n_x o_y Sin\theta + n_y o_x Sin\theta + o_y o_x \cos\theta + a_x a_y \\ n_y n_y Cos\theta - n_y o_y Sin\theta + n_y o_y Sin\theta + o_y o_y Cos\theta + a_y a_y \\ n_z n_y Cos\theta - n_z o_y Sin\theta + n_y o_z Sin\theta + o_y o_z Cos\theta + a_z a_y \\ 0 \end{bmatrix}$$

$$\begin{bmatrix} n_x n_z Cos\theta - n_x o_z Sin\theta + n_x o_x Sin\theta + o_z o_x \cos\theta + a_x a_z & 0 \\ n_y n_z Cos\theta - n_y o_z Sin\theta + n_z o_y Sin\theta + o_z o_y Cos\theta + a_y a_z & 0 \\ n_z n_z Cos\theta - n_z o_z Sin\theta + n_z o_z Sin\theta + o_z o_z Cos\theta + a_z a_z & 0 \\ 0 & 1 \end{bmatrix} \quad (5.14)$$

Simplifying the above relationship according to the following relationships

**(a)** The dot product of any row or column of the matrix C with any other row or column is zero, as the vectors are orthogonal;

**(b)** The dot product of any row or column of the matrix C with itself is 1 as the vectors are of unit magnitude;

**(c)** The z unit vector is the vector cross product of the x and y vector or

$$a = n \times o \quad (5.15)$$

which has components

$$a_x = n_y o_z - n_z o_y \tag{5.16.a}$$

$$a_y = n_z o_x - n_x o_z \tag{5.16.b}$$

$$a_z = n_x o_y - n_y o_x \tag{5.16.c}$$

and the *Versine*, is defined as $Vers\ \theta = (1 - Cos\ \theta)$

Therefore we have $k_x = a_x$ , $k_y = a_y$ and $k_z = a_z$

Now given any arbitrary rotational transformation, we can obtain an axis about which an equivalent rotation $\theta$ will produce the same result. We may equate $[R]$ to Rot(K,$\theta$) and get the following relation

$$\begin{bmatrix} N_x & O_x & A_x & 0 \\ N_y & O_y & A_y & 0 \\ N_z & O_z & A_z & 0 \\ 0 & 0 & 0 & 1 \end{bmatrix}$$

$$= \begin{bmatrix} K_xK_xVers\theta+Cos\theta & K_yK_xVers\theta-K_zSin\theta & K_zK_xVers\theta+K_ySin\theta & 0 \\ K_xK_yVers\theta+K_zSin\theta & K_yK_yVers\theta+Cos\theta & K_zK_yVers\theta-K_xSin\theta & 0 \\ K_xK_zVers\theta-K_ySin\theta & K_yK_zVers\theta+K_xSin\theta & K_zK_zVers\theta+Cos\theta & 0 \\ 0 & 0 & 0 & 1 \end{bmatrix} \tag{5.17}$$

Solving the above matrices ; we know $K_x^2 + K_y^2 + K_z^2 = 1$ , therefore we can get;

$$\begin{aligned} N_x+O_y+A_z+1 &= (K_x^2+K_y^2+K_z^2)Vers\theta+3Cos\theta+1 \\ &= 1+2Cos\theta \end{aligned} \tag{5.18}$$

Therefore we get

$$Cos\theta=(N_x+O_y+A_z-1)/2 \tag{5.19}$$

$$O_z-A_y=2K_xSin\theta \tag{5.20.a}$$

$$A_x-N_z=2K_ySin\theta \tag{5.20.b}$$

$$N_y-O_x=2K_zSin\theta \tag{5.20.c}$$

By squaring both the sides of equations (5.20.a) , (5.20.b) and (5.20.c) , we get

$$4Sin\theta^2(K_x^2+K_y^2+K_z^2) = (O_z-A_y)^2+(A_x-N_z)^2+(N_y-O_x)^2 \tag{5.21}$$

$$Sin\theta = \left[\frac{(O_z-A_y)^2+(A_x-N_z)^2+(N_y-O_x)^2}{2}\right]^{0.5} \tag{5.22}$$

Therefore we get

$$Tan\,\theta = \left[\frac{(O_z-A_y)^2+(A_x-N_z)^2+(N_y-O_x)^2}{N_x+O_y+A_z+1}\right]^{0.5} \tag{5.23}$$

Thus we can calculate the value of $\theta$ if we all the nine unknown elements of the Rotational Transformation matrix [$R$ ]. Therefore we can calculate

$$K_x = \frac{O_z - A_y}{2\,Sin\theta} \tag{5.24.a}$$

$$K_y = \frac{A_x - N_z}{2\,Sin\theta} \tag{5.24.b}$$

$$K_z = \frac{N_y - O_x}{2\,Sin\theta} \tag{5.24.c}$$

When the angle of rotation is very small, the axis of rotation is physically not well defined due to the small magnitude of both numerator and denominator in the above equations. If the resulting angle is very small, the vector $k$ should be renormalized to ensure that $|k| = 1$. When the angle of rotation approaches $180^0$ the vector $k$ is poorly defined by the above equations as the magnitude of the sine is again decreasing. When $\theta > 150^0$, the denominator of the above equations are less than one and as the angle increases to $180^0$ the rapidly decreasing magnitude of both numerator and denominator leads to considerable inaccuracies in the determining $k$ . At $\theta = 180^0$, the above equations are of the form $\frac{0}{0}$, yielding no information at all about physically well defined

vector $k$ . Equating the diagonal elements of the equation we can derive the following relations.

$$K_x^2 Vers\theta + Cos\theta = N_x \tag{5.25}$$

$$K_x = \pm \left[ \frac{N_x - Cos\theta}{1 - Cos\theta} \right]^{0.5} \tag{5.26.a}$$

Similarly we can find out

$$K_y = \pm \left[ \frac{N_y - Cos\theta}{1 - Cos\theta} \right]^{0.5} \tag{5.26.b}$$

$$K_z = \pm \left[ \frac{N_z - Cos\theta}{1 - Cos\theta} \right]^{0.5} \tag{5.26.c}$$

The largest component of $k$ defined by the equation (5.26.a) , (5.26.b) and (5.26.c) corresponds to the most positive component of $n_x$ , $o_y$ and $a_z$. For this largest element, the sign of the radical can be obtained from equation (5.20.a) , (5.20.b) and (5.20.c). As the sign of the angle of rotation $\theta$ must be positive, then the sign of the component of $k$ is determined from equations (5.20.a) , (5.20.b) and (5.20.c) must be the same as the sign of the left hand side of these equations. Thus we may combine the above information as follows

$$k_x = sgn\ (\ o_x - a_y\ ) \left[ \frac{n_x - Cos\ \theta}{1 - Cos\ \theta} \right]^{0.5} \tag{5.27.a}$$

$$k_y = sgn\ (a_x - n_z\ ) \left[ \frac{o_y - Cos\ \theta}{1 - Cos\theta} \right]^{0.5} \tag{5.27.b}$$

$$k_z = sgn(n_y - o_x\ ) \left[ \frac{a_x - Cos\theta}{1 - Cos\theta} \right]^{0.5} \tag{5.27.c}$$

where $sgn\ (e) = +1$ if e $\geq 0$ and $sgn\ (e) = -1$ if e $\leq 0$.

Only the largest element of $k$ is determined from equation (5.27.a) to (5.27.c) corresponding to the most positive element of $n_x$ , $o_y$ and $a_z$. The remaining elements are more accurately determined by the following equations formed by the by summing pairs of off-diagonal elements of equation (5.17)

$$n_y + o_x = 2\, k_x\, k_y Vers\ \theta \tag{5.28.a}$$

$$o_z + a_y = 2\, k_y\, k_z Vers\ \theta \tag{5.28.b}$$

$$n_z + a_x = 2\, k_z\, k_x Vers\ \theta \tag{5.28.c}$$

If $k_x$ is the largest in the equation (5.27) then from equation (5.28.a) and (5.28.c)

$$k_y = \frac{n_y + o_x}{2k_x Vers\,\theta} \tag{5.29.a}$$

$$k_z = \frac{a_x + n_z}{2k_x Vers\,\theta} \tag{5.29.b}$$

If $k_y$ is the largest in the equation (5.27) then from equation (5.28.a) and (5.28.b)

$$k_x = \frac{n_y + o_x}{2k_y Vers\,\theta} \tag{5.30.a}$$

$$k_z = \frac{o_z + a_y}{2k_y Vers\,\theta} \tag{5.30.b}$$

If $k_z$ is the largest in the equation (5.27) then from equation (5.28.c) and (5.28.b)

$$k_x = \frac{a_x + n_z}{2k_z Vers\,\theta} \tag{5.31.a}$$

$$k_y = \frac{o_z + a_y}{2k_z Vers\,\theta} \tag{5.31.b}$$

Therefore the axis of rotation is given by $K_x\, i + K_y\, j + K_z\, k$

We identify atleast three feature points on the ball and find out the coordinate of those three points ( w.r.t world coordinate system ) from 'split image' of first frame. Let the points be $(X_1,Y_1,Z_1)$ ,$(X_2,Y_2,Z_2)$ ,$(X_3,Y_3,Z_3)$respectively.

Now we consider the 'split image' of the second frame. From there we find out the coordinate of those three points ( w.r.t. world coordinate system) after rotation of angle $\theta$ about an axis $K_x i+K_y j+K_z k$ ( specified w.r.t world coordinate system transferred to the center of the ball). Let the coordinate of those points be $(X_1',Y_1',Z_1')$, $(X_2',Y_2',Z_2')$ and $(X_3',Y_3',Z_3')$ respectively .

Avoiding the subscripts we can write

$$[X, Y, Z, 1] \begin{bmatrix} N_x & O_x & A_x & 0 \\ N_y & O_y & A_y & 0 \\ N_z & O_z & A_z & 0 \\ 0 & 0 & 0 & 1 \end{bmatrix} = [X', Y', Z', 1] \qquad (5.32)$$

Each point ( X Y Z ) will produce three equations . Similarly three points will produce nine equations . We have nine Unknown parameters $N_x, N_y, N_z$ , $O_x, O_y, O_z$, $A_x, A_y, A_z$ respectively . Solving the following nine equations we can find out the Unknowns .

$$X_1N_x+Y_1N_y+Z_1N_z = X_1' \qquad (5.33.a)$$

$$X_2N_x+Y_2N_y+Z_2N_z = X_2' \qquad (5.33.b)$$

$$X_3N_x+Y_3N_y+Z_3N_z = X_3' \qquad (5.33.c)$$

Since there are errors in the estimation of the coordinate of the points $\overline{P}_i(X_i\ Y_i\ Z_i)$ and $\overline{P}_i'(X_i'\ Y_i'\ Z_i')$ for $i$ = 1 to n, number of feature points, from the images, the above procedure will result in incorrect evaluation of the nine elements of the rotation matrix [ $R$ ]. Presence of the sensor noise in the frames and the limited resolution of the camera are the main reasons for inaccurate estimation of the feature points. Once the correspondence of the feature points from frame to frame has been established, in order to obtain an optimal solution we propose the least square estimation of the

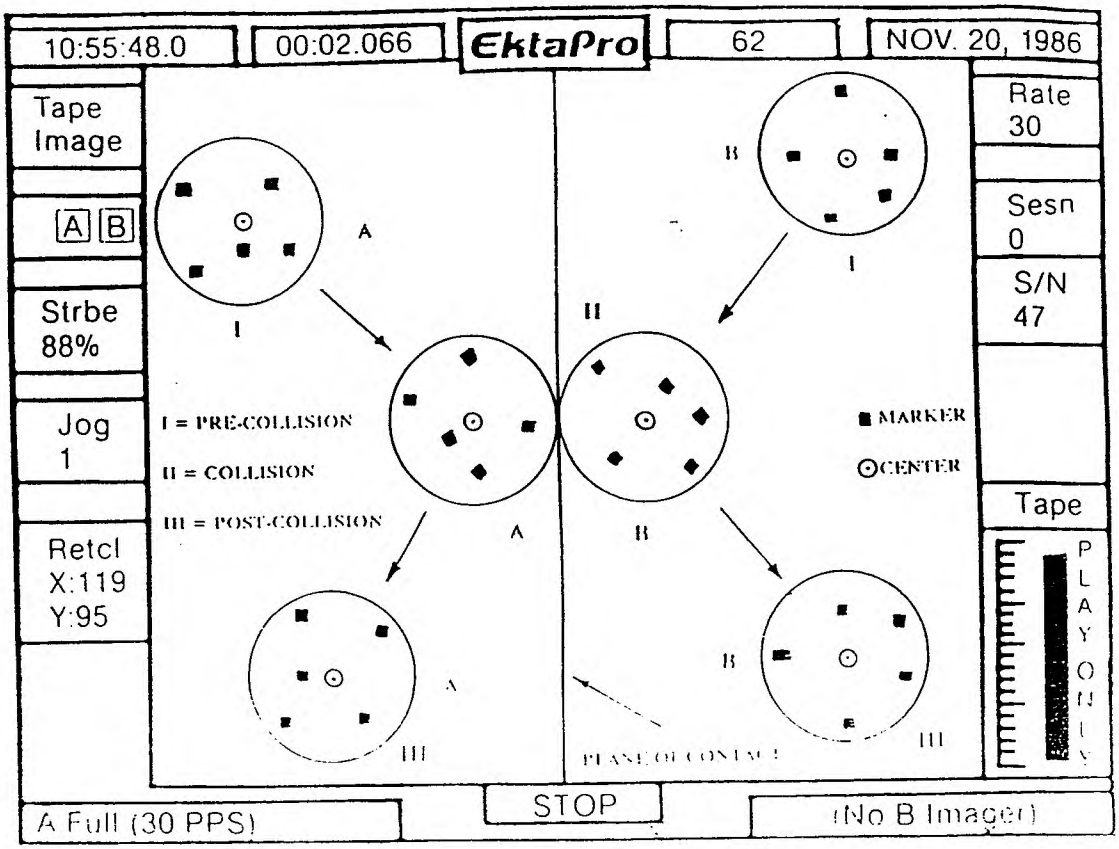


**Figure 5** View of Collision on Kodak Monitor

rotation parameters. Here we consider a set of points ( say n no of points) on each sphere and generate an overdetermined set of linear transformation equation. If $\overline{P}_i$ and $\overline{P}_i$ 'represents the coordinate of the same points on the ball obtained from two frames. There will be rotation and translation of the ball (i.e. the points ) in that period. If $[R]$ is the actual rotation transformation matrix, then

$$\overline{P}_i [R] = \overline{P}_i' \qquad \text{for i} = 1 \text{ to n} \tag{5.34}$$

Due to the error in the measurement of coordinate of the points $\overline{P}_i [R] - \overline{P}_i' \neq 0$

If $Er$ = Error, then

$$Er = [\overline{P}_i [R] - \overline{P}_i'] \text{ for i} = 1 \text{ to n.} \tag{5.35}$$

We represent total squared Error $F(p) = \sum_{i=1}^{n} Er \,.\, Er^T$ where p is function of the nine elements of the rotation matrix $[R]$ namely $(N_x, N_y, N_z, O_x, O_y, O_z, A_x, A_y, A_z)$.

So $F(p) = (X_i N_x + Y_i N_y + Z_i N_z - X_i')^2 + (X_i O_x + Y_i O_y + Z_i O_z - Y_i')^2$

$$+ (X_i A_x + Y_i A_y + Z_i A_z - Z_i')^2 \quad \text{for i} = 1 \text{ to } n \qquad (5.35.a)$$

Here we try to minimize this squared error w.r.t the nine parameters of the rotation matrix $[R]$ i.e. $(N_x \ldots A_z)$ and evaluate the optimal solution $p^*$. This is a nontrivial task because of the nonlinearity of the equations. Lagrange multipliers can be introduced and a solution can be found. However we minimize the function $F(p)$ by differentiating w.r.t. the nine parameters of the rotation matrix $[R]$ i.e.$(N_x \ldots A_z)$ and setting the first derivative $F(p)$ to 0. It has been shown in appendix C that the second derivative is greater than zero. Therefore the solution obtained minimizes the sum of the squared error $F(p)$.

$$\frac{\partial F(p)}{\partial N_x} = \sum_{i=1}^{n} 2(X_i N_x + Y_i N_y + Z_i N_z - X_i') \,.\, X_i = 0 \qquad (5.36.a)$$

$$\frac{\partial F(p)}{\partial N_y} = \sum_{i=1}^{n} 2(X_i N_x + Y_i N_y + Z_i N_z - X_i') \,.\, Y_i = 0 \qquad (5.36.b)$$

$$\frac{\partial F(p)}{\partial N_z} = \sum_{i=1}^{n} 2(X_i N_x + Y_i N_y + Z_i N_z - X_i') \,.\, Z_i = 0 \qquad (5.36.c)$$

$$\frac{\partial F(p)}{\partial O_x} = \sum_{i=1}^{n} 2(X_i O_x + Y_i O_y + Z_i O_z - Y_i') \,.\, X_i = 0 \qquad (5.36.d)$$

$$\frac{\partial F(p)}{\partial O_y} = \sum_{i=1}^{n} 2(X_i O_x + Y_i O_y + Z_i O_z - Y_i') \,.\, Y_i = 0 \qquad (5.36.e)$$

$$\frac{\partial F(p)}{\partial O_z} = \sum_{i=1}^{n} 2(X_i O_x + Y_i O_y + Z_i O_z - Y_i') \,.\, Z_i = 0 \qquad (5.36.f)$$

$$\frac{\partial F(p)}{\partial A_x} = \sum_{i=1}^{n} 2(X_i A_x + Y_i A_y + Z_i A_z - Z_i') \cdot X_i = 0 \tag{5.36.g}$$

$$\frac{\partial F(p)}{\partial A_y} = \sum_{i=1}^{n} 2(X_i A_x + Y_i A_y + Z_i A_z - Z_i') \cdot Y_i = 0 \tag{5.36.h}$$

$$\frac{\partial F(p)}{\partial A_z} = \sum 2(X_i A_x + Y_i A_y + Z_i A_z - Z_i') \cdot Z_i = 0 \tag{5.36.i}$$

We can rearrange the equation (5.36.a) to (5.36.c) in the following matrix form

$$\begin{bmatrix} \sum_{i=1}^{n} X_i^2 & \sum_{i=1}^{n} X_i Y_i & \sum_{i=1}^{n} X_i Z_i \\ \sum_{i=1}^{n} Y_i X_i & \sum_{i=1}^{n} Y_i^2 & \sum_{i=1}^{n} Y_i Z_i \\ \sum_{i=1}^{n} Z_i X_i & \sum_{i=1}^{n} Z_i Y_i & \sum_{i=1}^{n} Z_i^2 \end{bmatrix} \begin{Bmatrix} N_x \\ N_y \\ N_z \end{Bmatrix} = \begin{bmatrix} \sum_{i=1}^{n} X_i . X_i' \\ \sum_{i=1}^{n} Y_i . X_i' \\ \sum_{i=1}^{n} Z_i . X_i' \end{bmatrix} \tag{5.37}$$

Similarly rearranging the equations (5.36.d) to (5.36.f) in following matrix form we get

$$\begin{bmatrix} \sum_{i=1}^{n} X_i^2 & \sum_{i=1}^{n} X_i Y_i & \sum_{i=1}^{n} X_i Z_i \\ \sum_{i=1}^{n} Y_i X_i & \sum_{i=1}^{n} Y_i^2 & \sum_{i=1}^{n} Y_i Z_i \\ \sum_{i=1}^{n} Z_i X_i & \sum_{i=1}^{n} Z_i Y_i & \sum_{i=1}^{n} Z_i^2 \end{bmatrix} \begin{Bmatrix} O_x \\ O_y \\ O_z \end{Bmatrix} = \begin{bmatrix} \sum_{i=1}^{n} X_i . Y_i' \\ \sum_{i=1}^{n} Y_i . Y_i' \\ \sum_{i=1}^{n} Z_i . Y_i' \end{bmatrix} \tag{5.38}$$

Also rearranging the equations (5.36.g) to (5.36.i) we can obtain the following matrix

$$\begin{bmatrix} \sum_{i=1}^{n} X_i^2 & \sum_{i=1}^{n} X_i Y_i & \sum_{i=1}^{n} X_i Z_i \\ \sum_{i=1}^{n} Y_i X_i & \sum_{i=1}^{n} Y_i^2 & \sum_{i=1}^{n} Y_i Z_i \\ \sum_{i=1}^{n} Z_i X_i & \sum_{i=1}^{n} Z_i Y_i & \sum_{i=1}^{n} Z_i^2 \end{bmatrix} \begin{Bmatrix} A_x \\ A_y \\ A_z \end{Bmatrix} = \begin{bmatrix} \sum_{i=1}^{n} X_i . Z_i' \\ \sum_{i=1}^{n} Y_i . Z_i' \\ \sum_{i=1}^{n} Z_i . Z_i' \end{bmatrix} \tag{5.38}$$

It is clear from equations (5.36) , (5.37) and (5.38) that left and right side data matrices are easily computable from the coordinate of the feature points. Since the number of feature points (n) is not fixed and they are randomly marked on the sphere therefore the left data matrix will be a nonsingular i.e. invertible matrix. Therefore solving the equations (5.36) , (5.37) and (5.38) by premultiplying the inverse of the left data matrix to the right side of each of the equations we can compute nine elements of the rotation matrix [$R$ ] namely ($N_x, N_y, N_z, O_x, O_y, O_z, A_x, A_y, A_z$). Therefore the angle of rotation $\theta$ and three elements of the axis of rotation can be calculated by the equation (5.23) and equations (5.27.a) to (5.27.c) from the computed values of ($N_x \ldots A_z$).

The angular velocity ( $\omega$ ) is calculated by devising the angle of rotation ( $\theta$ ) by the time difference $\Delta$t between the two frames. However we need to evaluate the velocity at any particular instant before and after collision. Therefore we calculate the angular velocity of the spheres between two cosecutive pair of frames, all are at equal intervals and take the average to evaluate the instantaneous angular velocity at the intermediate frame.

# CHAPTER 5
# ACCURACY OF THE METHOD

## 5.1 Accuracy of Rotation Estimation

The proposed algorithm has been tested with actual data for the evaluation of rotation between two frames and compared with the known actual rotation. Measured rotation are provided to the sphere and computed according to the proposed algorithm from 1° to 7° at the step of 1° and checked for the accuracy. The results are shown in the figure 7 below.

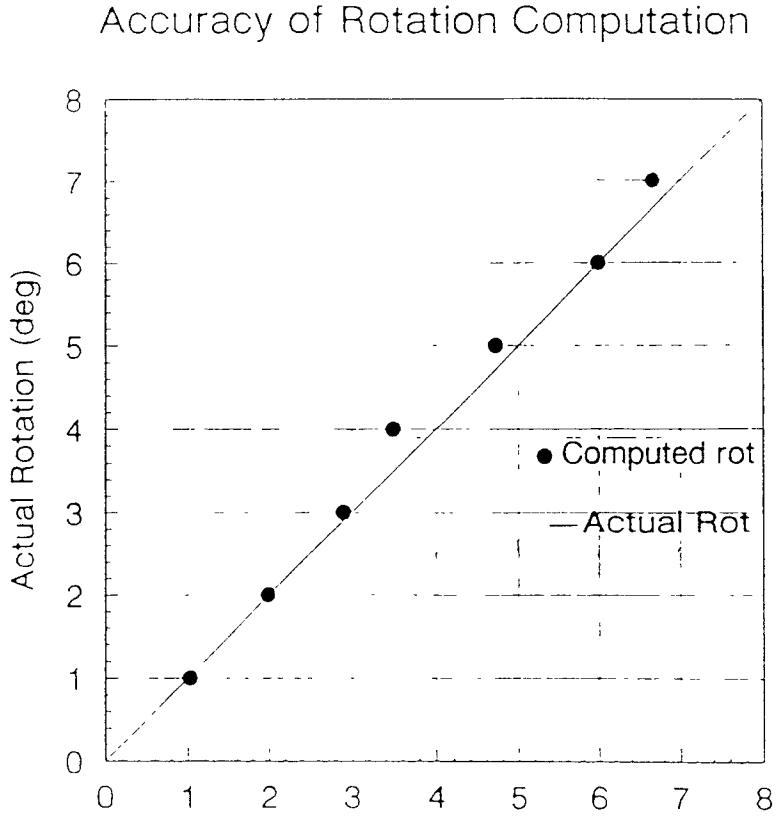


**Figure 6** Accuracy of Rotation Computation

## 5.2 Accuracy Estimation With Simulated Data

The proposed algorithm has been checked with simulated data for accuracy of rotation estimation. To evaluate the performance of the proposed method we perturbed the simulated data of the coordinate of the feature points by two sets of uniform random noise, first between 0.0 and 1.0 and second 0.0 to 0.5. The results of the computations are shown in the table 1 below. Normal computation yields to very close result to the actual rotation. The % error in the computation of the angle of rotation even with uniform random noise has never exceeded 2.0%. It may also be noticed that the axis of rotation evaluated also very closely approximates the ideal value. This proves the robustness of the algorithm against the possible error that creeps in while extracting the coordinate of the feature points from the image.

| | Angle of Rotation in degree | % Error in Computation | The Axis of Rotation $K_x i + K_y j + K_z k$ | | |
|---|---|---|---|---|---|
| | | | $K_x$ | $K_y$ | $K_z$ |
| Actual Rotation | 6.5 | - | 0.19 | 0.11 | 0.9756 |
| Calculated Rotation | 6.499394 | 0.0093 | 0.18927 | 0.111078 | 0.975504 |
| WithUniform noise 0.0 - 1.0 | 6.396028 | 0.8362 | 0.1993996 | 0.118358 | 0.972777 |
| WithUniform noise 0.0 - 0.5 | 6.445646 | 1.5996 | 0.21079 | 0.125927 | 0.969556 |
| Actual Rotation | 7.0 | - | 0.11 | 0.23 | 0.96695 |
| Calculated Rotation | 7.049199 | -0.7028 | 0.115392 | 0.228958 | 0.965282 |
| WithUniform noise 0.0 - 1.0 | 7.042138 | -0.602 | 0.131194 | 0.240072 | 0.960187 |
| WithUniform noise 0.0 - 0.5 | 7.037627 | -0.5375 | 0.124501 | 0.235044 | 0.962728 |
| Actual Rotation | 8.75 | - | 0.13 | 0.13 | 0.982955 |

| | | | | | |
|---|---|---|---|---|---|
| Calculated Rotation | 8.747318 | 0.0307 | 0.129339 | 0.129339 | 0.983455 |
| Uniform noise 0.0 -1.0 | 8.730437 | 0.2236 | 0.143497 | 0.143497 | 0.978706 |
| Uniform noise 0.0 -0.5 | 8.743148 | 0.0783 | 0.138465 | 0.137063 | 0.980859 |

Table 1. Results of Rotation estimation with simulated data

## 5.3 Accuracy vs Number of Feature Points

It is found with simulated data that if we increase the number of feature points (n) correspondence from frame to frame the accuracy of rotation estimation increases considerably. Since there are nine parameters of the rotation matrix require to be evaluated for the estimation of the angle and axis of rotation therefore at least same 3 feature points (i.e. 3 x 3 =9 coordinate values) correspondence are necessary between two successive frames. The more the number of feature points (n) correspondence the closer is the result to ideal value. The following table shows the output.

| | Angle of Rotation in degree | Axis of Rotation ( $K_x i + K_y j + K_z k$) | | |
|---|---|---|---|---|
| | | $K_x$ | $K_y$ | $K_z$ |
| Actual Rotation | 30.0 | 0.0 | 0.0 | 1.0 |
| 3-point correspondence | 29.561202 | - 0.059610 | - 0.001800 | 1.018056 |
| 4-point correspondence | 30.110158 | 0.020890 | 0.014379 | 1.008732 |
| 5-point correspondence | 30.095560 | 0.030215 | 0.013220 | 1.000801 |

| | | | | |
|---|---|---|---|---|
| 6-point correspondence | 30.049070 | 0.027804 | 0.012133 | 1.000122 |
| Actual Rotation | 6.00 | 0.0 | 1.0 | 0.0 |
| 3-point correspondence | 6.154007 | -0.110059 | 0.986416 | 0.119105 |
| 4-point correspondence | 5.779399 | -0.102239 | 0.991132 | 0.094127 |
| 5-point correspondence | 5.999426 | -0.11839 | 0.994905 | 0.101415 |

Table 2. Accuracy of Rotation evaluation with number of feature points correspondenc

# CHAPTER 6
# RESULTS AND DISCUSSION

## 6.1 Essence of The Experimentation

The experiment has been carried out on the setup shown in the figure 2 where two Teflon spheres are released at the same instant under gravity from the top of the two plastic tubes with the help of two solenoid triggering arrangement and allowed to collide in free space. The event of collision is imaged by the Kodak Ektpro 1000 video imaging system and the gray level image data is downloaded to a computer. By application of several image processing and edge detection operators on the image data, the position (coordinate) on the monitor, of the spheres and the markers on them are extracted from three frames each immediately before and after collision. From these position information the pre- and post-collision $\frac{v_s}{v_n}$ are calculated according to the algorithm explained in chapter iv. The rotational and linear coefficient of restitution ($\beta$ & $e$) are also evaluated from these data too.

The variation of pre-collision kinematics are achieved by changing the angle the tubes make with the horizontal (may be defined as 'tube angle' ). However, both the tubes should be equally inclined to ensure that the collision occurs. It has been observed during experiment that even a difference of $1^0$ between two tube angles results in no impact. The timing of the release of the spheres is the key element that determines whether the collision will occur. Since both the spheres are released under gravity, at very small tube angle the spheres will be merely dropped from the tubes instead of being projectiled to collide. It has been possible to carry out the

experiment at tube angle as low as $10^0$. If the tube angle is very high ( $>65^0$ ) the low height of the point of contact of the spheres is the constraint against the image to be grabbed. Also the mirror image goes out of the scene of collision.

## 6.2 Results of The Experiment

Experiment has been carried out at different tube angle settings, between $10^0$ and $65^0$. The results of the experiment is shown in the table below.

| Tube Angle in degree | Pre-Collision $(\frac{v_s}{v_n})$ | Post -Collision $(\frac{v_s}{v_n})$ | Normal Coefficient of Restitution ($e$) | Rotational Coefficient of Restitution ($\beta$) |
|---|---|---|---|---|
| 10 | 0.714907 | - 0.077257 | 1.132434 | -0.15480 |
| 15 | 0.258790 | - 0.217381 | 0.849218 | -0.71334 |
| 25 | 0.262297 | - 0.221256 | 0.902174 | -0.761011 |
| 35 | 0.156177 | - 0.109610 | 0.968966 | -0.68005 |
| 45 | 0.184295 | -0.1351841 | 0.670699 | -0.80441 |

Table 3 Results of the Experiment

Though the experiment has been carried out more number of times, in most of the other sessions the image of the collision were not good enough to extract the feature point coordinates through edge detection or the automatic correspondence could not be established from frame to frame. The rotational coefficient of restitution is found out to be in the range of -0.76. However more experimentation is necessary to substantiate the result. It may be noticed that the normal coefficient of restitution ($e$) at $10^0$ is incorrect.

The reason for erratic reasult is explained below. The normal and rotational coefficient of restituion ($e$ and $\beta$) are dependent on evaluation of pre- and post-collision relative surface velocity ($v_s$) and relative normal velocity ($v_n$). It may be

interesting to note the $v_s$ and $v_n$ are besed on the following expressions. At the instant of impact between two spheres the unit vector along the line joining the center of the spheres is determined as $\hat{r_{ab}} = \frac{r_b - r_a}{||r_{ab}||}$ where $r_a$ and $r_b$ are the 3-dimensional position of the center of the spheres w.r.t. the world coordinate frame. The relative velocity before and after collision is evaluated as $V_{ab} = V_b - V_a$ and $V_{ab}' = V_b' - V_a'$ where prime indicates the post-collision condition. The relative normal velocity or the component of relative velocity before and after collision along $\hat{r_{ab}}$ direction is expressed by $v_n$ and $v_n'$ are obtained as follows $v_n = \hat{r_{ab}} . V_{ab}$ and $v_n' = \hat{r_{ab}} . V_{ab}'$. Therefore it is evident that the calculation of normal coefficient of restitution ($e$) and rotational coefficient of restitution ($\beta$) are entirely dependent on how accurately we can evaluate the sphere center coordinates because thereafter the evaluation is pure arithmatic. However we observe the table of ($x$,$y$,$z$) coordinate of the sphere centers at subsequent frames w.r.t. the monitor of visilog system obtained through edge detection on image data as shown below.

| Frame No. | Normal Image | | | | Mirror Image | | | |
|---|---|---|---|---|---|---|---|---|
| | Sphere A | | Sphere B | | Sphere A | | Sphere B | |
| | X | Y | X | Y | X | Z | X | Z |
| 478 | 96 | 123 | 152 | 110 | 94 | 57 | 152 | 54 |
| 481 | 100 | 126 | 146 | 113 | 97 | 55 | 148 | 53 |
| 484 | 105 | 130 | 144 | 116 | 103 | 56 | 144 | 53 |
| Impact 487 | 107 | 132 | 140 | 118 | 106 | 57 | 137 | 53 |
| 490 | 104 | 139 | 144 | 119 | 103 | 56 | 142 | 53 |
| 493 | 101 | 145 | 147 | 120 | 99 | 55 | 145 | 51 |
| 496 | 97 | 150 | 148 | 122 | 98 | 57 | 146 | 52 |

Table 4 Sphere Center coordinates

It is assumed that the mirror image is obtained through reflection, by setting the mirror at $45^0$ to the plane of image sensor therefore the x-coordinate of both normal

and mirror image is supposed to be equal. However it is noticed for both the spheres A and B that the x-coordinate is not only different between normal and mirror image in each frame, the difference in x-coordinate varies from frame to frame.

Since from frame to frame the change in coordinate of the center of the spheres in terms of pixel value is restricted to 1 to 4 pixels therefore an error of 1 pixel in calculation of coordinate of the center will result in at least 25 % error in translation evaluation. It is relevent to mention that an error of 1 pixel in evaluation sphere center coordinate will result in $\frac{1000}{3}$ or 333.33 pixels per sec. error in velocity determination. The normal component of relative velocity $v_n$ is obtained by dot product of $V_{ab}$ and $\hat{r_{ab}}$ . It is evident here the x-component of $\hat{r_{ab}}$ is more predominant amongst all three elements. Therefore any error in the evaluation of x-coordinate of sphere center will be magnified in the calculation of $v_n$.

The rotation or the angular velocity $\omega_a$ and $\omega_b$ affects only the calculation relative surface velocity $v_s$. The expressions for calculation of $v_s$ are detailed below.

$$V_t = V_{ab} - v_n \,.\, \hat{r_{ab}} \tag{6.1}$$

$$V_s = V_t + \frac{\sigma}{2} \,.\, \hat{r_{ab}} \, x \, \omega_a + \frac{\sigma}{2} \,.\, \hat{r_{ab}} \, x \, \omega_b \tag{6.2}$$

$$v_s = \frac{V_s . V_s}{||V_s||} = ||V_s|| \tag{6.3}$$

| Tube angle setting | The Sphere checked | From frame No. | To frame No. | Angle of Rotation evaluated | The Axis of Rotation | | |
|---|---|---|---|---|---|---|---|
| | | | | | $K_x$ | $k_y$ | $K_z$ |
| | | 481 | 484 | 13.8718 | 0.1523 | 0.2333 | 0.9555 |
| | | 484 | 487 | 15.4087 | -0.1573 | 0.1914 | 0.9479 |
| | Left | 487 | 490 | 9.08634 | 0.4308 | 0.054 | 0.9005 |
| 10 | | 490 | 493 | 8.5222 | 0.0925 | 0.0562 | 0.9964 |

| | | | | | | | |
|---|---|---|---|---|---|---|---|
| | Right | 481 | 484 | -10.6618 | -0.0542 | -0.5812 | 0.8806 |
| | | 484 | 487 | -17.0268 | 0.0780 | 0.2988 | 0.9322 |
| | | 487 | 490 | -19.1026 | -0.0011 | -0.2305 | 0.9844 |
| | | 490 | 493 | -18.2863 | 0.0050 | -0.0370 | 0.9962 |

Table 5 Rotation evaluated from actual Experiment

It may be observed in the above table the angle and the axis of rotation are consistent and closely approximates the physical movement evaluated through eye estimation. The left sphere has +ve angle of rotation while the right sphere rotate -ve direction. The axis of rotation evaluated between two frames close to the expected value. The $k_z$ element is close to unity. Since the squared error in the evaluation of marker coordinates are minimized therefore the angle and axis of rotation are evaluation performs better.

The inaccuracy in the estimation of the coordinates may be due to the one or more of the following reasons.

First, since the 2-dimensional coordinate of the sphere center and the feature points obtained by projection on the imager, there is possibility of being image sensor not parallel to the plane of collision. Consequently, the projected points will have incorrect coordinate on monitor.

Second, due to limited resolution of the camera each pixel represents considerable length in space i.e. high scale factor. As a result, any error in estimation of coordinates of the sphere center or the markers through image processing will be magnified by the scale factor.

Third, the assumption of the experiment that two spheres remain on one vertical plane befor and after collision may not be the fact. Through the mirror being set at $45^0$ to the vertical plane of collision the movement along the depth (z-direction) is observed from the change z-coordinate. However the movement along z-direction

seems to be inconsistent. It may be noticed in Table 4 the z-coordinate of the mirror image of the sphere A changes erratically. Moreover the mirror image is incomplete or could not be captured by the imager for higher tube angle settings (from $35^0$ onward ). This is due to the fact that when tubes make higher angles with the horizontal, the collision occurs further away from the mirror and the mirror image does not come within the field of view of the camera.

It is clear that the determination of coordinate of sphere centers with high accuracy is essential since the evaluation of collision parameters are very sensitive to the coordinate of the sphere centers.

The value of pre- and post-collision $(\frac{v_s}{v_n})$ is plotted in the graph next page. The curve fitted corresponds to the sliding solution. However more experimental data are necessary to establish the slope of the curve.

## 6.3 Discussion on Limitations of The Experiment

A few of the constraints of this experiment are discussed here.
First, since the spheres are allowed to collide under gravity therefore the variation of pre-collision velocity is entirely dependent on the change in tube angle. Therefore it is not possible to observe collision behavior over a wide range of conditions.

Second, the motion parameters are estimated from the change in the position and orientation of the spheres in the frames through edge detection and image analysis. Therefore to ensure good (with minimum noise ) image, lighting should be appropriately diffused over the entire field of view of the imager. It is best to fix the lighting during each session by trying several times in different settings.

Third, the linear velocity is determined by observing the change in the position of the sphere center. While the angular velocity is evaluated by tracking a few randomly marked feature points on the sphere. Therefore care has to be taken to ensure that the feature point under observation should not get projected on the edge of the sphere in the image or occlude itself (i.e. does not go out of the scene). This has been achieved by setting the spheres at the top of the tube, with randomly marked feature points on only one side of the sphere, facing the camera. As a result, the axis of rotation of the sphere (i.e. markers) could be restricted, such that it does not cause the feature points occlude by itself during motion.

## 6.4 Future Direction of Research

More number of times the experiment should be carried out and observe the coordinate of the sphere centers and also should be checked by manual method. The following precision techniques needs to be incorporated to improve the accuracy of the entire procedue.

Since the evaluation of the collision parameters in the long run depends on the estimation of the 2-dimensional coordinate of the feature points from frame to frame, therefore determination of sphere center coordinate with subpixel accuracy is essential. Smoothing of locus of the sphere center is necessary for better velocity evaluation.

There has to be a reliable arrangement of observing the movement of the spheres in depth for better evaluation of pre and post-collision kinematics. The best solution is one more imager. Then two imagers could be set to collect two orthogonal views

with narrow field of view restricted to the region of collision. That in turn will also improve the resolution of the system and the accuracy of measurement.

The rotation parameters has been estimated through least square fitting of coordinates of two sets of feature point sets. The underlying assumption of this technique is that all the error in extracting the coordinate of feature points are only restricted to the second set of feature points. However this is unrealistic since there can be possible errors in the estimation of coordinate of feature points in both data sets. The application of Total least square estimation, will be appropriate and is expected to yield improved results in rotation calculation.

# APPENDIX - A
# AN OVERVIEW OF THE MECHANICS OF COLLISION

## A. 1 Introduction

Before we begin our study of collision parameters of particles it is important to know the background of the principles of dynamics based on which the expressions of different types of collision has been derived. The expressions derived here were taken from Walton [6] and presented here for the sake of completeness.

## A. 2 Derivation of Expressions

Let us consider two rigid particles of mass $m_1$ and $m_2$ moving linearly towards each other with the velocities $v_1$ and $v_2$ respectively. If the velocities after collision be $v_1$' and $v_2$' respectively then from the conservation of linear momentum assuming no external impulse force

$$m_1v_1' + m_2v_2' = m_1v_1 + m_2v_2 \qquad \text{(A.1)}$$

The relative velocity separation $v_r'$ and relative velocity of approach $v_r$ are defined as $v_r' = v_1 - v_2$ and $v_r = v_1 - v_2$. We define the coefficient of restitution e such that $v_r' = ev_r$ or $e = v_r'/v_r$ where e = 1 for perfectly elastic and e = 0 for perfectly plastic particles.

From the definition of coefficient of restitution and Eq. A.1 we can derive

$$v_1' = \frac{(m_1 - em_2)v_1}{(m_1+m_2)} + \frac{m_2(1+e)v_2}{(m_1+m_2)} \qquad \text{(A.2.a)}$$

and

$$v_2' = \frac{m_1(1+e)v_1}{(m_1+m_2)} + \frac{(m_2-em_1)v_2}{(m_1+m_2)} \qquad \text{(A.2.b)}$$

Assuming the frame of reference moving with the center of the mass of the system, we can define the velocity of the center of the mass ofthe system before and after collision as

$$v_c = \frac{(m_1v_1+m_2v_2)}{(m_1+m_2)} \qquad \text{(A.3.a)}$$

and

$$v_c' = \frac{(m_1v_1'+m_2v_2')}{(m_1+m_2)} \qquad \text{(A.3.b)}$$

Therefore the Equ. (A.2.a) and (A.2.b) can be expressed as

$$v_1' = \frac{v_c - e\, m_2\, v_r}{(m_1+m_2)} = v_c - \frac{m_2\, v_r'}{(m_1+m_2)} \qquad \text{(A.4.a)}$$

and

$$v_2' = v_c + \frac{e\, m_1\, v_r}{(m_1+m_2)} = v_c + \frac{m_1\, v_r'}{(m_1+m_2)} \qquad \text{(A.4.b)}$$

Similarly the velocity of the particles before collision can be expressed as

$$v_1 = v_c + \frac{m_2\, v_r}{(m_1+m_2)} \qquad \text{(A.4.c)}$$

$$v_2 = v_c - \frac{e\, m_1\, v_r}{(m_1+m_2)} \qquad \text{(A.4.d)}$$

**Lun and Savage Hard Sphere Collision operator**

We refer to the figure where point c refer to the point of contact of particle1 and 2 before contact. If the diameter of the particles be $\sigma$ and $r_{12} = (r_2-r_1)$ and

$\hat{r_{12}} = r_{12}/|r_{12}|$ then the velocity of the contact point of each of the particles can be represented as

$$V_{c_1} = \dot{r}_1 + \frac{d}{dt_{xyz}}(\frac{\sigma}{2}\hat{r_{12}}) \tag{A.5.a}$$

since r $c_1 = r_1 + \frac{\sigma}{2}\hat{r_{12}}$ and $rc_2 = r_2 - \frac{\sigma}{2}\hat{r_{12}}$ and $|\hat{r_{12}}|$ similarly

$$V_{c_2} = \dot{r}_2 - \frac{d}{dt_{xyz}}(\frac{\sigma}{2}\hat{r_{12}}) \tag{A.5.b}$$

Let $g_{12} = V_{c_1} - V_{c_2}$ and $V_1 = \dot{r}_1$ and $V_2 = \dot{r}_2$ and $\omega_{12} = \omega_1 + \omega_2$

Therefore

$$g_{12} = V_1 - V_2 - \frac{\sigma}{2}(\hat{r_{12}} \times \omega_{12}) \tag{A.6}$$

We know the component of relative velocity in the $\hat{r_{12}}$ direction after collision reduces by "e", coefficient of restitution. Therefore we get

$$\hat{r_{12}} . V_{21}' = -e\,\hat{r_{12}} . V_{12} \tag{A.7}$$

The reduction in angular velocity component in t -direction after collision due to $\beta$ can be expressed as

$$\hat{r_{12}} \times g_{12}' = -\beta(\hat{r_{12}} \times g_{12}) \tag{A.8}$$

The value of $\beta = 1$ when the colliding particles are perfectly rough and $\beta = -1$ for perfectly smooth particles.

The normal component $V_n$ and the tangential component $V_t$ of the relative velocity are expressed as

$$V_n = V_{12} . \hat{r_{12}} \tag{A.9}$$

$$V_t = \hat{r_{12}} \times (V_{12} \times \hat{r_{12}}) = V_{12} - V_n \tag{A.10}$$

So the relative surface velocity at the contact point in the tangential direction is expressed as

$$V_s = V_t + \frac{\sigma}{2}\hat{r_{ab}} \times (\omega_1 + \omega_2) \tag{A.11}$$

The unit vector in the direction of surface velocity $\hat{k_s}$ is evaluated as

$$\hat{k_s} = \frac{V_s}{|V_s|} \tag{A.12}$$

and the tangential component of relative surface velocity

$$v_s = V_s \cdot \hat{k_s} \tag{A.13}$$

Therefore from the definition of coefficient of normal restitution e, we get,

$$e = -\frac{v_n}{v_n} \tag{A.14}$$

Hence the velocity of center of mass immediately before and after collision Equ. A.5.a and A.5.b are represented as

$$V_{cn} = \frac{m_1 V_1 \hat{r_{12}} + m_2 V_2 \hat{r_{12}}}{(m_1 + m_2)} \tag{A.15.a}$$

and

$$V_{cn}' = \frac{m_1 V_1' \hat{r_{12}} + m_2 V_2' \hat{r_{12}}}{(m_1 + m_2)} \tag{A.15.b}$$

Referring to Equ. (A.1) we can write

$$V_1 = (V_a \cdot \hat{r_{ab}}) \cdot \hat{r_{ab}} \qquad V_1' = (V_a' \cdot \hat{r_{ab}}) \cdot \hat{r_{ab}}$$
$$V_2 = (V_b \cdot \hat{r_{ab}}) \cdot \hat{r_{ab}} \qquad V_2' = (V_b' \cdot \hat{r_{ab}}) \cdot \hat{r_{ab}}$$

Now we calculate the change in normal velocity of particle a $\Delta V_{na}$

$$-\Delta V_{na} = V_{na} - V_{na}' = (V_a \cdot \hat{r_{ab}})\hat{r_{ab}} - (V_a' \cdot \hat{r_{ab}})\hat{r_{ab}}$$

Through derivation we can obtain

$$\Delta V_{na} = \frac{(1+e)m_b(V_b - V_a)\,\hat{r}_{ab}\,\hat{r}_{ab}}{(m_a + m_b)}$$

$$\Delta V_{na} = \frac{m_b(1+e)V_n}{(m_b + m_a)} \qquad \text{(A.16.a)}$$

Similarly we can derive

$$\Delta V_{nb} = V_{nb}' - V_{nb} = (V_b' \,.\, \hat{r}_{ab})\hat{r}_{ab} - (V_b \,.\, \hat{r}_{ab})\hat{r}_{ab}$$

Therefore we get the change in normal direction velocity of particle b $\Delta V_{nb}$ a

$$\Delta V_{na} = - m_a(1+e)V_n/(m_b + m_a) \qquad \text{(A.16.b)}$$

The rotational restitution coefficient $\beta$ is defined as

$$\beta = \frac{-v_s'}{v_s} = \frac{-V_s' \,.\, k_s}{V_s \,.\, k_s} \qquad \text{(A.17)}$$

where $v_s'$ and $v_s$ are defined in Equ.(A.10) and (A.11) as

$$V_s = V_t + \frac{\sigma}{2}\hat{r}_{ab} \times (\omega_a + \omega_b) \quad \text{and} \quad V_t = \hat{r}_{ab} \times (V_{12} \times \hat{r}_{ab}) = V_{ab} - V_n$$

and

$$V_s' = V_t' + \frac{\sigma}{2}\hat{r}_{ab} \times (\omega_a' + \omega_b') \quad \text{and} \quad V_t' = \hat{r}_{ab} \times (V_{12}' \times \hat{r}_{ab}) = V_{ab} - V_n..$$

Here $\omega_a'$ and $\omega_b'$ are the rotational velocity of the particles a and b.

From the theory of conservation of angular momentum about the contact point; we know

$$\sum (AngularMomentum)_{pre\_collision} = \sum (AngularMomentum)_{post\_collision}$$

For particle of mass $m_a$

$$-\frac{\sigma_a}{2}\hat{r}_{ab} \times m_a V_{ta} + I_0\,\omega_a = -\frac{\sigma_a}{2}\hat{r}_{ab} \times m_a V_{ta}' + I_0\,\omega_a' \qquad \text{(A.18.a.)}$$

$$m_a \frac{\sigma_a}{2} \hat{r_{ab}} \text{ x } (V_{ta}' - V_{ta}) = I_0 (\omega_a' - \omega_a)$$

$$\Delta \omega_a = m_a \sigma_a (\hat{r_{ab}} \text{ x } \Delta V_{ta})/2I_0 = 2(\hat{r_{ab}} \text{ x} \Delta V_{ta})/K \sigma_a \qquad \text{(A.19.a)}$$

Similarly for the particle of mass $m_b$

$$\frac{\sigma_b}{2} \hat{r_{ab}} \text{ x } m_b V_{tb} + I_0 \omega_b = \frac{\sigma_b}{2} \hat{r_{ab}} \text{ x } m_b V_{tb}' + I_0 \omega_b' \qquad \text{(A.18.b)}$$

$$\Delta \omega_b = m_b \sigma_b (\hat{r_{ab}} \text{ x } \Delta V_{tb})/2I_0 = 2(\hat{r_{ab}} \text{ x} \Delta V_{tb})/K \sigma_b \qquad \text{(A.19.b)}$$

The theory of conservation of linear momentum in tangential direction can be expressed as

$$\sum (LinearMomentum)_{pre\_collision} = \sum (LinearMomentum)_{post\_collision}$$

Therefore

$$m_a V_{ta} + m_b V_{tb} = m_a V_{ta}' + m_b V_{tb}' \qquad \text{(A.20)}$$

$$\Delta V_{tb} = -\frac{m_a}{m_a} \Delta V_{ta} \qquad \text{(A.21)}$$

### A.2.1 Rolling Solution

The rotational restitution coefficient is defined as

$$v_s . \beta = v_s' \quad or \quad \beta . V_s . k_s = V_s' . k_s' \qquad \text{(A.22)}$$

If we recall the definition of surface velocity

$$V_s = V_t + \frac{\sigma}{2} \hat{r_{ab}} \text{ x } \omega_a + \frac{\sigma}{2} \hat{r_{ab}} \text{ x } \omega_b \qquad \text{(A.23)}$$

Therefore

$$\Delta V_s = \Delta V_t + \frac{\sigma}{2} \hat{r_{ab}} \text{ x } \Delta \omega_a + \frac{\sigma}{2} \hat{r_{ab}} \text{ x } \Delta \omega_b \qquad \text{(A.24)}$$

where

$$\Delta V_s = V_s' - V_s \qquad \text{(A.24.a)}$$

and $\Delta\,\omega_a$ and $\Delta\,\omega_b$ are given by equation (A.19a) and (A.19b)as

$$\Delta\,\omega_a = m_a\sigma_a(\hat{r_{ab}}\ \mathrm{x}\,\Delta\,V_{ta})/2I_0 = 2(\hat{r_{ab}}\,\mathrm{x}\Delta\,V_{ta})/K\,\sigma_a \qquad \text{(A.25.a)}$$

and

$$\Delta\,\omega_b = m_b\sigma_b(\hat{r_{ab}}\ \mathrm{x}\,\Delta\,V_{tb})/2I_0 = 2(\hat{r_{ab}}\,\mathrm{x}\Delta\,V_{tb})/K\,\sigma_b \qquad \text{(A.25.b)}$$

We recall

$$V_t = V_{ta} - V_{tb} \quad \text{and} \quad V_t' = V_{tb}' - V_{ta} \qquad \text{(A.26)}$$

and

$$\Delta\,V_{ta} = V_{ta}' - V_{ta} \quad \text{and}\ \Delta\ V_{tb} = V_{tb}' - V_{tb} \qquad \text{(A.27)}$$

Therefore

$$\Delta\ V_t = V_t' - V_t = \Delta\,V_{tb} - \Delta\,V_{ta} \qquad \text{(A.28)}$$

Therefore from equations (A.19 a), (A.19.b), (A.24) and (A.27) we derive

$$\Delta\,V_s = \Delta\,V_{tb} - \Delta\,V_{ta} + m_a\,\sigma_a^2(-\Delta\ V_{ta})/4I_0 + m_b\,\sigma_b^2\,\Delta\ V_{tb}/4I_0 \qquad \text{(A.29)}$$

Also from the definition of rotational restitution coefficient ( $\beta$ ), we get

$$\Delta\ V_s = V_s' - V_s \quad = -(1+\beta)\,V_s \qquad \text{(A.30)}$$

Substituting equations (A.29) and (A.21) into ( A.28 ), we get

$$-(1-\beta)V_s = \frac{-m_a}{m_b}\ \Delta\,V_{ta} - \Delta\,V_{ta} - m_a\sigma_a^2\,\Delta\,V_{ta}/4I_0 + m_b\,\sigma_b^2\,(-\frac{m_a}{m_b})\Delta\,V_{ta}/4I_0 \qquad \text{(A.31)}$$

Simplifying the above expression, we get

$$(1+\beta)V_s = \Delta\,V_{ta}\,[\,(1+\frac{m_a}{m_b})\,(1+\frac{1}{K})] \qquad \text{(A.32)}$$

where $K = \frac{I_0}{mr^2}$ and $I_0 = \frac{2}{5}mr^2$. So $K = \frac{2}{5}$. Here $m_a\frac{\sigma_a^2}{4I_0} = \frac{1}{K} = \frac{5}{2}$

Hence we derive

$$\Delta V_{ta} = m_b(1+\beta)V_s K/(m_a + m_b)(1+K) \quad \text{(A.33)}$$

$$\Delta V_{tb} = -m_a(1+\beta)V_s K/(m_a + m_b)(1+K) \quad \text{(A.34)}$$

$$\Delta \omega_a = 2m_b(1+\beta)(\hat{r_{ab}} \times V_s)/(m_a + m_b)\,\sigma_a\,(K+1) \quad \text{(A.35)}$$

$$\Delta \omega_b = 2m_a(1+\beta)(\hat{r_{ab}} \times V_s)/(m_a + m_b)\,\sigma_b\,(K+1) \quad \text{(A.36)}$$

### A.2.2 Sliding Solution

For sliding solution tangential force is always friction limit during the entire motion.

$$(Tangential\ Impulse) = \mu\ .\ (Normal\ Impulse) \quad \text{(A.37)}$$

We calculate the change in the tangential velocity of both the spheres due to the collision and express as

$$V_{ta}' - V_{ta} = \Delta V_{ta} = \mu\ |V_{na}|\hat{k_s} \quad \text{(A.38.a)}$$

$$V_{tb}' - V_{tb} = \Delta V_{tb} = \mu\ |V_{nb}|\hat{k_s} \quad \text{(A.38.b)}$$

where $\hat{k_s} = \frac{V_s}{|V_s|}$ is defined as the unit vector in the direction of unit surface velocity.

Substituting the equations (A.4.a), (A.4.b), (A.4.c) and (A.4.d) in the above relations we get

$$\Delta V_{ta} = \mu m_b\,(1+e)\ |V_n|\hat{k_s}/(m_a+m_b) \quad \text{(A.39.a)}$$

$$\Delta V_{tab} = -\mu m_a\,(1+e)\ |V_n|\hat{k_s}/(m_a+m_b) \quad \text{(A.39.b)}$$

Similarly we can calculate the change in the rotational velocity of each of the spheres

$$\Delta \omega_a = \frac{\sigma_a}{2I_a}\mu m_a m_b(1+e)|V_n|(r_{ab} \times \hat{k_s})/(m_a + m_b) \quad \text{(A.40.a)}$$

$$\Delta \omega_b = \frac{\sigma_b}{2I_b} \mu m_a m_b (1+e) |V_n| (r_{ab} \text{ x } \hat{k_s}) / (m_a + m_b) \qquad \text{(A.40.b)}$$

Calculation of Rotational Restitution Coefficient for Sliding solution

We refer to equation (A.32) and express as

$$(1+\beta^*) V_s = \Delta V_{ta} [ (1 + \frac{m_a}{m_b}) (1 + \frac{1}{K})]$$

where $\beta^*$ represents the rotational restitution coefficient resulting from sliding contact. Substituting $\Delta V_{ta}$ from equation (A.33) in the above expression we get

$$(1+\beta^*) V_s = \mu(1+e) |V_n| (1+\frac{1}{K}) \hat{k_s} \qquad \text{(A.41)}$$

or

$$\beta^* = -1 + \mu(1+e) \frac{|V_n|}{|V_s|} (1+\frac{1}{K}) \qquad \text{(A.42)}$$

This may noted that calculation of $\beta^*$ is independent of the mass of the particles. Whenever the value of $\beta^* > \beta_0$ the rolling solution, with fixed value of $\beta = \beta_0$ is employed to calculate the post collision velocities.

# APPENDIX - B
# SALIENT FEATURES OF KODAK EKTAPRO 1000 MOTION ANALYZER

## B.1 Introduction

The Kodak Ektapro1000 Motion Analyzer is designed to be a valuable addition to the scientist's and engineer's problem solving tool kit. The menu driven keypad and the interactive display make evaluating the most difficult motion related problems simple. The most important aspect is that the live setup feature allows the user to ensure the image to be recorded is sufficient to solve the motion problem. The images recorded are immediately available for analysis.

## B.2 Constituent Elements

The Kodak Ektapro1000 camera and motion analyzer system is composed of following basic components

(1) Imager (2) Monitor (3) Processor (4) Keypad connected to the processor (5) Intensified imager (6) Cassettes etc.

### B.2.a Imager

Light enters the imager through the lens and is converted into an electrical signal or video signal. The video signal corresponds precisely to the variation in intensity and spatial relationships of the image captured by the lens. The intensity of light coming from different objects in the image varies the amplitude of the video signal. The time difference between video amplitude changes represents the spatial relationship between the objects. The video signal created in the imager is amplified and

processed so that it can be transmitted through the cable to the processor. The most important component of the imager is the sensor board.

### B.2.a.1 Sensor

The Sensor is a 'solid state imaging array' has thousands of photo capacitive cells that can convert light focused by the lens into measurable electrical charges. The amount of charge stored in each cell, called "pixel", varies according to the intensity of the light received and is actually an analog for that amount of light. In the sensor, the charge stored by each cell is picked up once per frame by the scanning process. While scanning the charge collected from each cell in the array one after another. As each cell releases its charge, a new charge begins to accumulate for the next scan, based on the light that it receives. The video signal is nothing more than a linear sequence of varying amount of charge from each pixel scanned. Kodak camera has the pixel array organized into a structure containing 240 columns and 192 rows. Since each scanning cycle must read 46,800 pixels before starting over again, it restricts rate to about 60 frames per sec. To achieve a frame rate of 1000 frames per sec it is necessary to scan the array 16 times faster. The Kodak system achieves the speed increase by scanning 16 rows of pixels simultaneously. The scanning sequence reads the first pixels in each of sixteen rows simultaneously and then reads the next pixel in each of the same 16 rows. This process continues until the 16 rows have been output from column 1 through 240 of the pixel array. This requires 16 output channels that are switched internally from one group of 16 rows to the next group as the scanning of the array proceeds. It takes 12 blocks to make up a single frame with16 pixel rows in each block. The video signal resulting from the scanning process is amplified by the rest of circuitry to a suitable level for receipt by the processor.

The remaining circuitry consists of (a) Two Analog Sample board (b) High speed digital board (c) Low speed digital board (d) Viewfinder etc.

### B.2.b Processor

The processor card bin contains eleven printed circuit cards required to control the system and is configure from keypad to operate in the live, record or play mode.

### B.2.b.1 Live Mode

When operating in live mode, the processor monitor displays the picture that will be recorded. The picture composition exposure and focus are all exactly as they appear when a recording is played back. The essential electronics of live mode are the

(a) Cable Interface Board: This board facilitates the routing of imager video from imager to the Analog imager interface

(b) Image Intensifier Board: This board displays the imager and combination of imager to be displayed and recorded.

(c) Analog/Digital Converter: This board converts the analog video from the analog imager interface board to a digital signal. The digitized video signal is stored in frame buffer by the frame writer board in the same way that a personal computer stores data in its memory.

(e) Frame Buffer: It has storage capacity of 1.5 million bits of digital information permitting storage of four complete frames of video image.

(f) Graphics Board: This board reads frame buffer and System control unit and generates standard video picture with Data-frame border.

### B.2.b.2 Record Mode

In the record mode the processor continues to put the image on the monitor exactly as in live mode, however, the tape transport is commended to move tape at user selected speed and the modulator an record boards are turned on sending the video signal to the record head. The speed at which the tape moves while recording varies according to the frame rate. At 1000 frames per sec the tape moves at 250 inches per sec. The basic operation requires the following components.

Modulator: It imager video into frequency modulated signal.

Record: The record board provides the energy required to drive the record head.

### B.2.b.3 Play Mode

During play mode to view a recorded event in slow motion, tape is first rewind to the beginning of the recording and then moved at 7.5 inches per sec. by 'Tape transport' system which provides the mechanics and electronics to control tape speed and direction. As a result frame rate in play mode is always at 30 frames per sec. The replay function can be used to review the latest recording. The processor enters the play mode when the tape transport signals that it is moving the tape forward at the correct speed.

Demodulator: The demodulator board converts the frequency modulated signal from reproduce head back to a video signal.

Analog/Digital Converter: The Analog to Digital Converter now uses the output of the demodulator instead of the signal coming from the imager.

### B.2.c Timing and System Control

The video from the imager and the processor that go on inthe card bin during live and record mode must be synchronized in time. Video being played from tape must also be synchronized with the playback circuitries. Basic constituent of the electronics are

(a) TDC: The Timing and data controller generates the clock waveforms that synchronizes both the record electronics and the imager.

(b) Imager Interface Digital: This board passes the timing information from TDC to the imager. This also passes signal to the video signal board.

(c) SCU: The System Control unit is the board that carries the microprocessor that is managing the entire system.

(d) SCUM: The System Control unit Memory board cntains contains the rest of the circuitry required to support the operation of the microprocessor on the SCU. It also contains the communication circuitry for the keypad and the transport.

## B.3 Lenses and Its Selection

The purpose of a lens in motion analysis videography is to capture enough light to see the action, keep the action in focus and produce an image that of proper size to resolve the motion problem. The parameters which will be adjusted are the f/stop, focus. There are various types of lenses are used for different purposes, namely (a) Normal lenses (b) Wide Angle lenses (c) Telephoto lenses (d) Macro lenses (e) Fixed focal length lenses (f) Zoom lenses etc. The ability of lens to capture light affects motion analysis in two respects. First, if a lens can capture more light, we can

# KODAK EKTAPRO 1000 MOTION ANALYZER MENU CHART

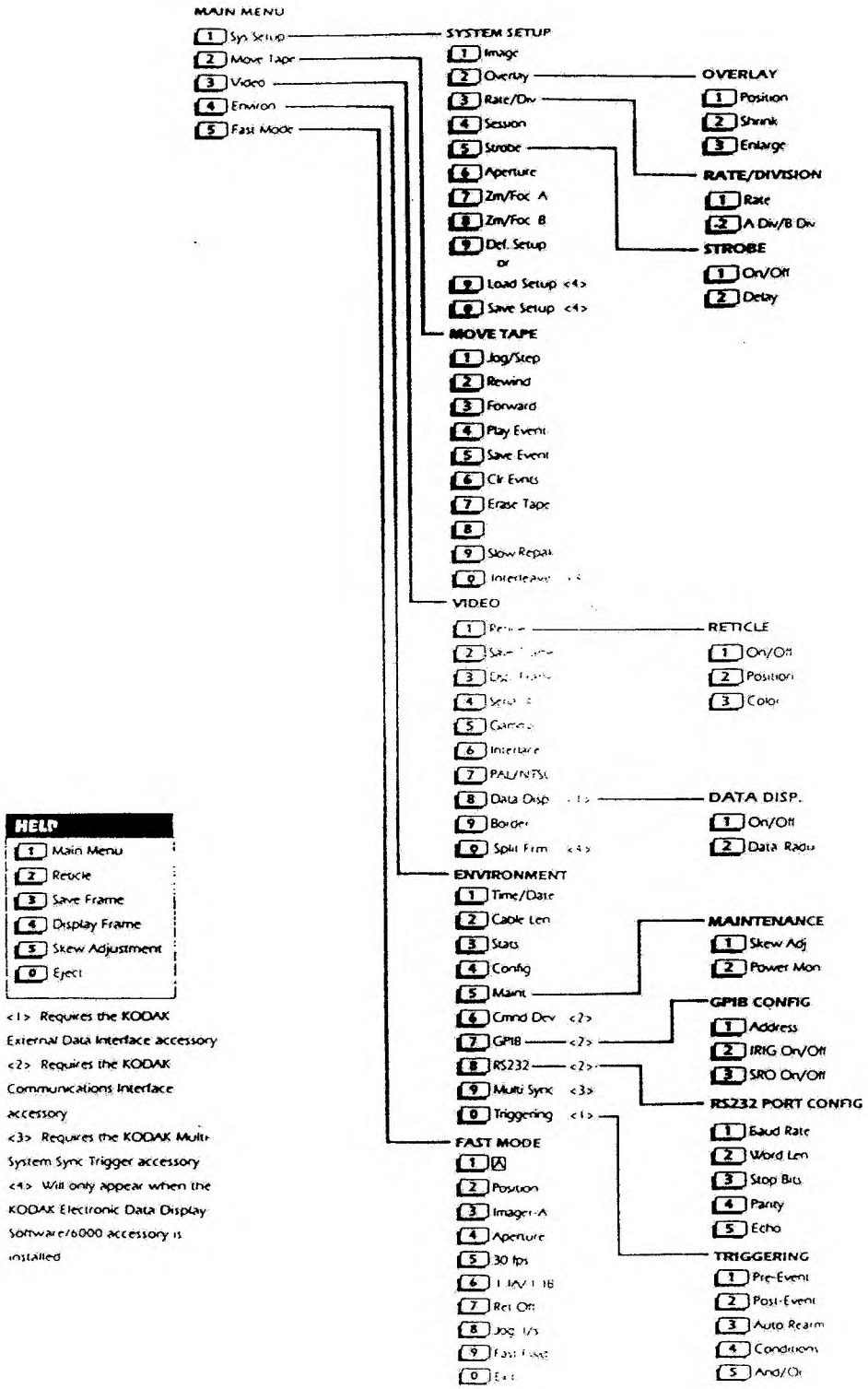


<1> Requires the KODAK External Data Interface accessory

<2> Requires the KODAK Communications Interface accessory

<3> Requires the KODAK Multi-System Sync Trigger accessory

<4> Will only appear when the KODAK Electronic Data Display Software/6000 accessory is installed

set the system to a higher frame rate for the same amount of light. Second, with better light gathering ability, the lens aperture can be decreased with a desirable increase in the depth of field. For this, an electronically controllable variable focal length Zoom lense is most appropriate. There are two issues to be considered for lens selection in a particular application. First is field of view i.e. the vertical and horizontal dimension of the scene that frames the action one's interest. It depends on focal length (depth of field) and distance of action from lens. Second issue determines which lens can resolve smallest object movement for motion analysis problem

## B.4 Keypad Control

The Keypad connected to the Kodak Ektapro1000 motion analyzer has a large crystal display and a number of control keys that allows the user to manage all of the system functions. The Chart in the prvious page shows the whole menu structure with all its functions and the respective key, being identified by the number, to be pressed to produce the desired effect.

## B.5 Intensified Imager

The intensifier assembly functions as an electronic shutter and light amplifier. It increases the imager's ability to capture events in low light or to reduce blurring of objects moving through the field of view vary fast. The amount of light is controlled by the 'Gain' and the 'Gate' determines the time (in the order of 10 $\mu$sec) of electronic shutter opening during each frame. These two controller are properly adjusted to noise and blur free images. Another advantage of the intensifier is the control over the depth of field. With the reduction in lens aperture the object remain in focus over greater

distance however the less light received by the imager can be compensated by the intensifier. The life of photosensitive surface of intensifier is limited to $5 \times 10^8$ effective exposures and can get permanently damaged if the scene illumination exceed 10,000 Lux even for a sec. The system has in built automatic protection arrangement of overload limit and time-out control.

## B.6 Important Features of Video Imaging System

Few of the most useful features of the Kodak Ektapro1000 video imaging system are

[1] This video system can record the event in a video cassaet in a rate as high as 1000 frames per sec. Each frame can be split into as many as six pictures. The same event can be played back at a rate 30 frames per sec.

[2] Exposure level can be controlled from menu driven keypad.

[3] Images from two different cameras can be can be recorded simultaneously.

[4] Elapsed time display and built in reticle of the system allows immediate measurement of motion parameters quick and accurate.

[5] While playing the recorded event, we can jog the frames at any rate from 1 to 8 frames per sec. or advance 1 frame at a time in step mode.

[6] Replay function facilitates the play back of immediately recorded event.

[7] The record lockout dial prevents accidental recording over a recorded tape.

[8] Control from the keyboard, as well as by an external digital signal, of the entire setup makes the operations very flexible.

[9] The image captured is grey level and transferrable to other computer for further processing.

[**10**] This system provides a video output signal compatible with NTSC or PAl standard video recording signal formats. Therefore recorded event can be downloaded into normal video cassette and displayed on TV monitor.

# APPENDIX - C
# AN OVERVIEW OF THE LEAST SQUARE ERROR ESTIMATION METHOD

If we consider solving a list of inconsistent nonhomogeneous linear equations ($i=1$ *to* $n$) represented as

$$A \,.\, x = b \qquad \text{(C. 1)}$$

the least square solution among all x is a vector $x^*$ for which $||Ax - b||_2$ is minimal. Here $||\alpha||_2$ refers to the euclidean norm evaluated by the expression $[\sum_{i=1}^{n} |\alpha_i|^2]^{0.5}$. We try to solve the equation (C. 1) where $A \in R_{mx\,n}$, $x \in R_{nx\,1}$ and $b \in R_{mx\,1}$. We know that the system of equation has a solution if and only if $r(A) = r(A|b)$ i.e. the vector $b$ is in the range of the matrix $A$. From mathematical stand point the solvability of $A \,.\, x = b$ is completely answered by this requirement. However in many practical linear transformation problem, the assumption of $r(A) = r(A|b)$ is no longer valid and we attempt to determine an approximate solution of the equation (C.1) by employing the principle of least squares.

The theory is extensively used in establishing linear mathematical relationship amongst two or more sets of experimental or observable data. It has relevance in many computer vision applications, notably the estimation of the rotation parameters of rigid object using 3-dimensional point correspondence [55] and determination of relative attitude of a rigid object with respect to a reference frame [56].

To begin with, we define

$$r(x) = A.x - b \tag{C.2}$$

for any $x \in R_{nx1}$. The vector $r(x)$ is called the residual vector or the noise vector. Thus $r(x)$ is the amount of error that comes into the picture when we take $x$ as an approximate solution of equation (C.1). Least square solution will have the property of minimizing the $||r(x)||_2^2$. From the theory of inner product of vectors we know,

$$\begin{aligned} ||r(x)||_2^2 &= (A.x - b, A.x - b) \\ &= (A.x - b)^T (A.x - b) \\ ||r(x)||_2^2 &= x^T A^T A x - 2x^T A^T b + b^T b \end{aligned} \tag{C.3}$$

The above expression is a scalar quantity which we can denote $f(x)$.

$$f(x) = x^T A^T A x - 2x^T A^T b + b^T b \tag{C.4}$$

Now the element of the matrix $A$ are determined to minimize the value $f(x)$ i.e. the sum of the square of the deviations. This is the method of least square error.

Many mathematical problems are concerned with finding the maximum or the minimum value of function w. r. t. one or more variables. It also happens that the problem reduces to finding the greatest or least value of a function over neighborhood $N(x_0)$ of a point $x_0$,

$$N(x_0) = [x \mid x_0 - \varepsilon < x < x_0 - \varepsilon] \tag{C.5}$$

where $\varepsilon > 0$ and $N(x_0)$ is contained in the domain of the function.

The greatest (least) value (if there is one) of a function on the entire domain is called the absolute maximum (minimum) alternatively known as extremes. But the function $f(x)$ is said to have a relative maximum at point $x = a$ of the domain if there exist a neighborhood $N(a)$ such that $f(a) > f(x)$ for each $x \in N(a)$. Similarly, a function

$f(x)$ is said to have a relative minimum value at a point $x = a$ of the domain of $f(x)$ such that there is neighborhood $N(a)$ where $f(a) \leq f(x)$ for each $x \in N(a)$.

One of the important application of ordinary and partial derivatives is the determination of the relative maximum or minimum of a function over a domain. From the theory of maxima and minima we know, If $y = f(x)$ and $A\ (a, f(a))$ is a point on the graph such that $f'(a) = 0$ and $f''(a) < 0$ then A is the relative maximum and it occurs at $x = a$.

Similarly, if $f'(a) = 0$ and $f''(a) > 0$ then $A$ is relative minimum. The test fails if $f''(a) = 0$.

Let $h \in R_{n\,x\,1}$ and $h \neq 0$. We can express the first derivative as $f'(x)$ from equation (C.4) as

$$f'(x) = \lim_{h \to 0} \frac{[f(x+h) - f(x)]}{h} \tag{C.6}$$

$$\begin{aligned} f(x+h) - f(x) &= h^T A^T A h + h^T A^T A\, x + x^T A^T A h - 2h^T A^T b \\ &= h^T A^T A h + 2h^T (A^T A x - A^T b) \end{aligned} \tag{C.7}$$

since $x^T A^T A h$ is a scalar quantity and

$$x^T A^T A h = (x^T A^T A h)^T = h^T A^T A x$$

and $(A+B)^T = A^T + B^T$. Obviously at limit, when $h \to 0$, we have to stop at positive h and we can evaluate x by setting $f'(x) = 0$. Similarly we can show that $f''(x) > 0$. The second derivative can be expressed as $f(x)$ in terms of $x$ and $x+h$ as

$$f''(x) \approx \frac{f(x+h) - 2f(x) + f(x-h)}{h^2} \tag{C.8}$$

Evaluating the functions $f(x+h)$ and $f(x)$ and rearranging the terms it can be shown that

$$f''(x) = \frac{2h^T A^T Ah}{h^2} = \frac{2(Ah)^T (Ah)}{h^2} = \frac{2\,(A\,.\,h)^2}{h^2} > 0.$$

Therefore the solution $x$ calculated from equation (C.7) by setting $f'(x) = 0$ will give us the least square solution.

Alternatively this can be explained from the definition of relative minimum (maximum), where $f(x+h) - f(x)$ must be of the same sign for all small values of vector h. However the sign of the expression (C.7) depends on the term $h^T(A^T Ax - A^T b)$. But this term will change sign with $h$ if $(A^T Ax - A^T b) \neq 0$. Hence $f(x)$ to have an minimum value, it is required to be $(A^T Ax - A^T b) = 0$. If this condition is satisfied $f(x)$ has a minimum at $x = x^*$ and can be evaluated from the expression

$$A^T Ax^* = A^T b \tag{C.9}$$

Therefore the least square solution of the nonhomogeneous and inconsistent system of linear equations $A\,.\,x = b$ is also obtainable from the solution of nonhomogeneous but consistent system of linear equations $A^T Ax = A^T b$.

# REFERENCES


1. German, R. M. Particle Packing Characteristics, Metal Powder Industries Federation Princeton, NJ (1989).

2. Jenkins, J.T. "Balance Laws and Constitutive Relations for Rapid Flows of Granular Materials." *Constitutive Models of Deformation*, SIAM (1987).

3. Nakagawa, M. "Anisotropic Theory of Rapidly Deforming Granular flow." *Theoretical and Applied Mechanics*, 37 :(1989): 183-194.

4. Richman, M. W. and Chou, C. S. "Boundary Effects on Granular Shear Flows of Smooth Disks." *ZAMP* 39:(1988): 886-901.

5. Lun, C.K.K. and Savage, S. B. *J. Appl. Mech.* 54: (1987): 42-53 .

6. Walton, O.R. "LLNL Granular Solids Flow Project Quarterly Report," UCID 20297-88-1, May 1988.

7. Walton, O. R. and Braun, R.L., "Viscosity, Granular-Temperature and Stress Calculations for Shearing Assemblies of Inelastic Spheres in Uniform Shear." *J. Rheol.* 30(5) (1986): 949-980 .

8. Walton, O. R. and Braun, R.L. "Stress Calculations for Assemblies of Inelastic Spheres in Uniform Shear." *Acta Mechanica* 63:(1986): 73-86 .

9. Walton, O.R., Kim. H. Rosato, A.D. "Microstructure and Stress Differences in Shearing Flows." *Mechanics Computing in 1990s and Beyond, Proceedings / EM Div/ASCE, Columbus, OH,* May 20-22, 1991.

10. Kim. H., Rosato, A.D. "Particle Simulations of the Flow of Smooth Spheres Between Bumpy Boundaries." *2nd. US / Japan Seminar on Micromechanics of GranlarMaterials, Clarkson University, Postdam, NY,* Aug. 5-9, 1991.

11. Maw, N., Barber, J. R., Fawcett, J.N."Role of Elastic Tangential Compliance in Oblique Impact."*ASME Journal of Lubrication Technology* 103,(1981): 74-80.

12. Drake, T.G. and Shreve, R. "High Speed Motion Picture of Nearly Steady Uniform Two DimensionaI Inertial Flow of Granular Material." *J. Rheology,* (1986): 981-993.

13. Chaudhari, S. and Chatterjee, S. "Motion Analysis of Homogeneously Deformable Object Using Subset Correspondence." *Pattern Recognition* 24 (1991): 739-745.

14. Horn, B.K.P. Robot Vision, The MIT Press, Cambridge, Mass.(1986).

15. Ballard, D. H. and Brown, C. M. Computer Vision, Prentice Hall, Englewood Clifford, NJ (1982).

16. Rangrajan, K. and Shah, M. "Establishing Motion Correspondence." CVGIP: Image Understanding 54 (1991): 56-73 .

17. Berne, B.J. Journal of Chem. Physics, 66, 7,(1977): 1745-1754.

18. Veseley, F.S. Molecular Physics, 41, 5,(1980): 959-1015.

19. Goldsmith, W. Impact, East Arnold Pub., London (1960).

20. Hawkins, G.W. "Simulation of granular Flow." in Mechanics of Granular Materials, New Models and Constitutive Relations, (1983): 305-312.

21. Campbell, C. S. and Brennen, C. E. "Computer Simulation of Granular Shear Flows." *J. Fluid Mech.* 151, (1985): 167-188.

22. Ullman, S. The Interpolation of Visual Motion, The MIT Press, Cambridge, Massachussates (1979).

23. Hildreth, E. C. The Measurement of Visual Motion. The MIT Press, Cambridge,Massachussates (1983).

24. Hung, T. S. (ed.) Image Sequence Processing and Dynamic Scene Analysis, Springer-Verlag, New York (1983).

25. Netravail, A. and Robbins, J. "Motion Compensation TV Coding: Part 1." *Bell Syst.emic Technical J,* vol. 58, 1979: 631-670.

26. Tsai, R. Y. and Huang, T. S. "Moving Image Restoration and Registration." *In Proced.ings IEEE Into. Conf. ASSP, Denver, CO,* Apr. 9-11, 1980.

27. Rocca, F. "TV Bandwidth Compression Utilizing Frame to Frame Correlation and Movement Compensation." Picture Bandwidth Compensation, T. S. Hung and O. J. Tretiak, Eds. London: Gordon and Breach, 1972.

28. Tsai, R. Y. and Huang, T. S. "Moving Image Restoration." presented at the *IEEE Computer Soc. Workshop on Comput. Anal. of Time Varying Imagery, PA,* Apr. 5-6, 1976.

29. Limb.,J. and J. Murphy, "Estimating Velocity of Moving Image in TV Signal" *Computer Graphics Image Processing*, vol. 4: (1975): 311-327.

30. Horn, B.K.P. and Schunck, B. G."Determinig Optical Flow." *AI Memo.* 572 MIT, Apr. 1980.

31. Cafforio, C. and Rocca, F. "Tracking Moving Objects In TV Images."*Signal Processing.*"vol. 1(1979): 133-140.

32. Schalkoff, R. J. "Algorithems for Real-time Automatic Video Tracking sytem."*Ph.D.dissertation*, Dep. Elec. Eng., Univ. VA Charlottesville, 1979.

33. Braunstein, M.L."Depth Perception Through Motion." New York: Academic, 1976.

34. Gibson, J. J. "The Perception of the Visual World." Boston, MA: Houghton and Mifflin,1950.

35. Roberts, L.G. "Machine Perception of 3-Dimensional Solids." in *Coputer methods in Image Analysis.* 1978.

36. Roach, J. W. and Agarwal, J. K."Determining The Movement of Objects from Sequences of Images." *IEEE Trans. Pattern Anal. Machine Intell.*, vol. PAMI-2 Nov. 1979.

37. Webb, J. A. and J. K. Agarwal,"Structure from Motion of Rigid and Jointed bodies." *International Conference on Artificial Intelligence*, Aug. 1981.

38. Nagel, H. N. and Neumann, B, "On 3-Dimensional Reconstruction from two Perspective Views." *in Proc. IJCAI 81,* vol. II, Aug. 1981.

39. Meiri, A. Zvi. "On Monocular Perception of 3-Dimensional Moving Objects." *IEEE Transaction Pattern Analysis Machine Itelligence*, PAMI-2, Nov. 1980.

40. Tsai, R.Y. and Huang, T. S. "Uniqueness and Estimation of 3-Dimensional Motion Parametrs of Rigid Objects with Curved Surfaces." *Proc. IEEE Conf. Computer Vision Pattern Recognition,* Miami Beach, FL, 24-29june 1986.

41. Castro, E. D. and Morandi, C, "Registration of Translated and Rotated Images using,Finite Fourier Transforms." *IEEE Trans. Pattern Anal. Mach. Intelligence,* PAMI 9 Sept. 1987.

42. Weng, J., T. S. Huang and Ahuga, N. "3-Dimensional Motion Estimation Un Standing and Predictionfrom Noisy Image Sequences ." *IEEE Trans. Pattern Anal. Machine Intelligence* PAMI-9 (1987): 370-389.

43. Whon, K. and S. L. Iu. "Estimation Of 3-dimensional Motion And Structure based On-temporally Oriented Approach With The Method Of Regression." *IEEE workshop on Visual Motion,* (1989): 21-30.

44. Whon, K. and S. L. Iu. "Recovery of 3-Dimensional motion of Single Particle." *Pattern Recognition,* vol. 24 (1991): 241- 251.

45. Badler, N. "Temporal Scene Analysis: Conceptual Descrcription of Object Motion." *Ph.D. dessertation, Univ. Toronto*, Toronto, Ont. Canada, TR80, 1975.

46. Lawton, D. T. "The Processing of Dynamic Images and the Control of the Robot Behaviour." *Ph.D. Dissertation, Univ. of Massachusetts* (1981).

47. Canny, J."A Computational Approach to Edge Detection."*IEEE Trans. Pattern Analysis Machine Intell.*, PAMI-8 (1986): 651-664.

48. Hough, P. V. C., "Method and Means for Recognizing Complex Patterns."*The US patent No.* 3069654.